Antisense oligonucleotides targeting translation inhibitory elements in 5′ UTRs can selectively increase protein levels

Xue-hai Liang[1,*], Hong Sun[1], Wen Shen[1], Shiyu Wang[1], Joyee Yao[1], Michael T. Migawa[2], Huynh-Hoa Bui[3], Sagar S. Damle[3], Stan Riney[3], Mark J. Graham[3], Rosanne M. Crooke[3] and Stanley T. Crooke[1]

[1]Department of Core Antisense Research, Ionis Pharmaceuticals, Inc., Carlsbad, CA, USA, [2]Department of Medicinal Chemistry, Ionis Pharmaceuticals, Inc., Carlsbad, CA, USA and [3]Department of Antisense Drug Discovery, Ionis Pharmaceuticals, Inc., Carlsbad, CA, USA

ABSTRACT

A variety of diseases are caused by deficiencies in amounts or activity of key proteins. An approach that increases the amount of a specific protein might be of therapeutic benefit. We reasoned that translation could be specifically enhanced using *trans*-acting agents that counter the function of negative regulatory elements present in the 5′ UTRs of some mRNAs. We recently showed that translation can be enhanced by antisense oligonucleotides (ASOs) that target upstream open reading frames. Here we report the amount of a protein can also be selectively increased using ASOs designed to hybridize to other translation inhibitory elements in 5′ UTRs. Levels of human RNASEH1, LDLR, and ACP1 and of mouse ACP1 and ARF1 were increased up to 2.7-fold in different cell types and species upon treatment with chemically modified ASOs targeting 5′ UTR inhibitory regions in the mRNAs encoding these proteins. The activities of ASOs in enhancing translation were sequence and position dependent and required helicase activity. The ASOs appear to improve the recruitment of translation initiation factors to the target mRNA. Importantly, ASOs targeting *ACP1* mRNA significantly increased the level of ACP1 protein in mice, suggesting that this approach has therapeutic and research potentials.

INTRODUCTION

Aberrant protein expression can cause diseases, and down regulation of specific protein expression via mechanisms such as antisense technology is now used clinically (1–5).

Many diseases, however, are caused by insufficient levels of functional proteins (6,7); therefore it would be beneficial to specifically increase the level of a protein. Several approaches have been developed to achieve this goal, such as delivery of expression constructs or mRNAs, suppression of repressive proteins or transcripts, modulation of splicing, or inhibition of the nonsense-mediated decay pathway to increase mRNA, and, therefore, protein levels (8–11). These approaches have limitations including challenges in the *in vivo* delivery of large DNA or RNA molecules and the fact that there are limited number of genes that can be controlled using these strategies (8,12–14). New methodology is thus needed that could be applied to more genes to increase protein expression, especially *in vivo*.

Translation is highly regulated and is responsive to many types of stimuli and physiological conditions (15–18). In eukaryotes, translation occurs predominantly in a cap-dependent manner, although cap-independent translation does occur and is often mediated by internal ribosome entry sites (IRES) (19–21). During translation, the eIF4F complex, containing eIF4E, eIF4G and eIF4A, binds to the 5′ m^7G cap. The helicase eIF4A may help to resolve structure formed within the 5′ end of the mRNA, facilitating the recruitment of other proteins (17,22,23). Next, the pre-formed 43S complex, which contains the 40S small ribosomal subunit (SSU), eIF2–GTP–tRNAiMet ternary complex, and other initiation factors, binds to the mRNA, generating the 48S pre-initiation complex (PIC) (17). The PIC then scans for the AUG start codon in a 5′ to 3′ direction (24,25). At the start codon, the initiator Met-tRNAi base pairs with the mRNA, and the 60S large subunit (LSU) joins to form the 80S ribosome, which initiates translation (23).

Translation initiation is a rate-limiting step in eukaryotic protein expression (17,18), and *cis*-acting elements present in the 5′ UTRs of mRNAs are known to modulate translation. These elements, such as upstream open reading

frames (uORFs), mRNA structures, and protein binding sites, can inhibit translation through different mechanisms (17,23,26,27). For example, translation of a uORF can inhibit translation initiation of the downstream primary ORF (pORF) encoding the main protein product. In addition, structures adopted by 5′ UTRs can inhibit translation initiation (22,28), though certain structures, like IRES, may increase translation under certain circumstances.

The existence of inhibitory elements in 5′ UTRs of certain mRNAs provides opportunities to increase specific protein production by inactivating these elements using *trans*-acting agents, such as antisense oligonucleotides (ASOs) that can sequence-specifically base pair with the mRNA. Indeed, we recently found that ASOs that bind to uORF regions but do not induce cleavage of the mRNA can increase levels of protein encoded by the downstream pORF in cells and in animals (29). This study confirmed that *trans*-acting ASOs, a class of agents that have been studied for >25 years for abilities to down-regulate protein expression (4), can specifically increase protein levels. As uORFs are only present in ∼50% of mammalian mRNAs (30,31) and some uORFs may not be inhibitory, this strategy is not applicable to all genes. To expand the repertoire of genes for which protein expression can be up-regulated, we evaluated the effects of ASO binding to other translation inhibitory elements in 5′ UTRs.

It has been suggested that ∼10% of cellular mRNAs contain atypically long 5′ UTRs, which tend to form stable secondary structures and in general, such structures inhibit translation (26,27,32,33). Sequences of many 5′ UTRs are predicted to form stable structures, including secondary structures and G-quadruplexes, that have been shown to inhibit translation (28,34–36). Disruption of these G-quadruplex structures by either small molecules or oligonucleotides has been reported to increase translation efficiency (35,37,38). On the other hand, secondary structure, as one of the two best studied 5′ UTR inhibitory elements (the other is uORF), can inhibit translation, as demonstrated three decades ago (27,39–43). In alignment with the inhibitory effect of 5′ UTR structures, a genome-wide study has shown that mRNAs with weakly folded 5′ UTRs have higher translation rates (28). Whereas in another study, it was found that a class of poorly translated mRNAs tend to have stable secondary structures within 5′ UTRs (34).

The inhibitory effect of the stem–loop structures has been demonstrated to be dependent on the thermodynamic stability and the position of the structure relative to the 5′ cap (40,42,44–48). For example, when a stem structure (–25 kcal/mol) was placed at positions +4 or +10 relative to the 5′ cap, translation efficiency was increased by 11- or 50-fold, respectively, relative to that when placed at position +1 (47). In addition, it has been found that when a stem-loop structure with –30 kcal/mol was placed at position +12, but not at +52, translation was significantly reduced (44). However, when a stronger stem structure (–61 kcal/mol) was placed even at position +72 relative to the cap, translation was still blocked.

Secondary structures at 5′ UTRs can inhibit the loading or scanning of the PIC, depending on the position and the thermodynamic stability (42,48). For instance, when a stem (–30 kcal/mol) was placed at positon +12 relative to the 5′

cap, but not at +52, mRNA association with the PIC was inhibited. However, when a stronger stem (–61 kcal/mol) was placed at position +72, the PIC bound the mRNA, but was stalled ahead of the stem structure (44). Other studies also confirmed that 5′ UTR stem structures near the cap inhibit binding of translation initiation factors, such as eIF4B, to the mRNAs (49). A working model has been established regarding the inhibitory effect of 5′ UTR secondary structures: a stem structure near the cap can inhibit the loading of the PIC to the mRNA, whereas a stem structure not proximal to the cap allows PIC binding, and once bound, the PIC is able to penetrate secondary structure if the thermodynamic stability of the structure is not too strong (32,33,44). Thus, disruption of these structures or interactions of mRNA regions with inhibitory proteins or other factors, should enhance translation and increase levels of proteins.

Here, we report that using ASOs targeting 5′ UTR inhibitory elements, including potential structured regions, we were able to significantly increase levels of protein encoded by five different genes in human and mouse cells. The ASOs are specific and act by enhancing translation, most likely due to increased recruitment of translation initiation factors to the target mRNA. Importantly, we showed that protein levels could be specifically increased in mouse using chemically modified ASOs targeting an inhibitory region in *ACP1* mRNA, suggesting that the approach described here has potential for therapeutic use.

MATERIALS AND METHODS

Antibodies and oligonucleotides

Antibodies, ASO sequences and chemical modifications, siRNA sequences and qRT-PCR primer probe set sequences are listed in Supplementary Information.

Cell culture and transfection

HEK293 and HeLa cells (from Life Technologies) and MHT cells (50) were grown in DMEM medium supplemented with 10% FBS at 37°C in an incubator with 5% or 8% CO_2. One day before transfection, cells were seeded at ∼60% confluency and incubated overnight. Transfection of ASOs was performed using Oligofectamine 2000 or RNAiMax (Life Technologies). For the RNASEH1 cleavage activity assay, cells transfected with ASO761919 were reseeded at ∼60% confluency, allowed to grow for 14 h, and then transfected again with an ASO targeting *Malat1* (ASO395254). RNA was harvested 4 h later. Transfection with siRNAs (3–5 nM final concentration) was performed using RNAiMax (Life Technologies). At 4 h or 24 h after siRNA transfection, cells were washed and transfected with ASOs. For the attenuation study using complementary oligonucleotide (Figure 1), HEK293 cells were co-transfected with ASO761919 and ASO927728 or with ASO761919 and ASO759704.

Western blotting

Cells were harvested using trypsin and washed once with PBS. Cell lysates were prepared in RIPA buffer (Pierce,
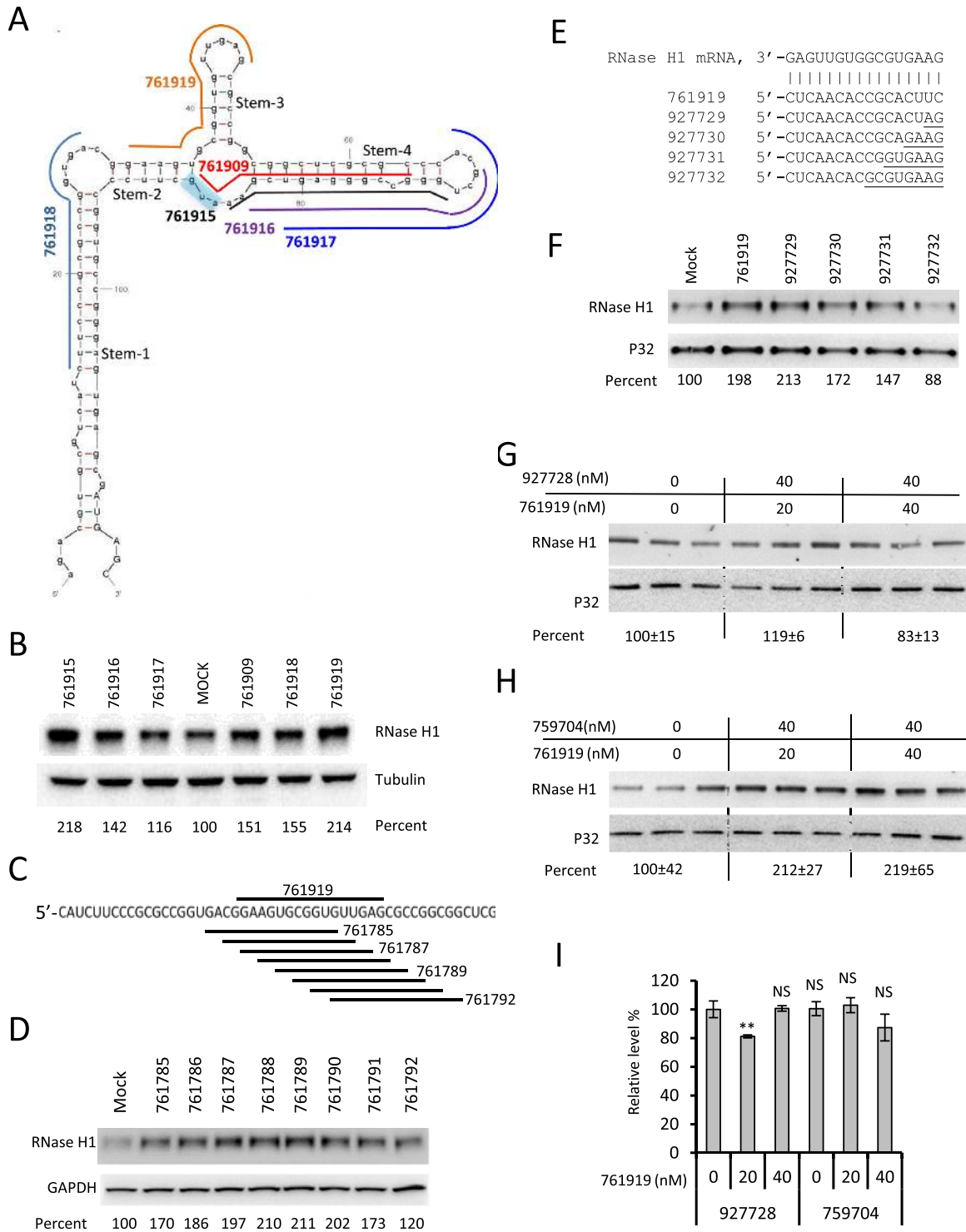
Figure 1. ASOs targeting the 5′ UTR of *RNASEH1* mRNA increase protein production. (**A**) Predicted secondary structure of the 5′ UTR of *RNASEH1*. The upper case letters indicate coding sequence. The start codon of the uORF is highlighted in blue. Binding sites for ASOs are indicated by lines. (**B**) Western blot for RNASEH1 in HeLa cells treated with indicated ASOs for 15 h at 25 nM. Numbers below the lanes are percentages of RNASEH1 protein relative to mock-treated cells; values are normalized to quantity of tubulin loading. (**C**) Schematic representation of ASO positions on *RNASEH1* bracketing active ASO761919. (**D**) Western blot for RNASEH1 in HeLa cells treated for 15 h with 25 nM indicated ASOs. GAPDH was used as a loading control. (**E**) Sequences of *RNASEH1* mRNA and ASOs with mismatches (underlined). (**F**) Western analysis for RNASEH1 protein in HeLa cells treated with 30 nM indicated ASOs for 10 h. P32 was detected as a loading control. (**G**) Western analyses for RNASEH1 in HeLa cells co-transfected with the *RNASEH1* ASO761919 and an ASO complementary to the *RNASEH1* ASO (ASO927728). ASO concentration 0 indicates mock transfection. (**H**) Western blot analyses for RNASEH1 in HeLa cells co-transfected for 10 h with ASO761919 and a control ASO759704. The mean values and standard deviations after normalization to P32 quantity are shown below the lanes. (**I**) qRT-PCR quantification of *RNASEH1* mRNA in cells treated with indicated ASOs. The error bars represent standard deviations from three experiments. *P*-values were calculated based on unpaired t-test. NS, not significant. **P < 0.01.

89901) and cleared by centrifugation at 10 000 × g for 10 min at 4°C. Proteins (20–40 μg/lane) were separated on 4–12% gradient SDS-PAGE, transferred to membrane, and blotted with primary and secondary antibodies. Proteins were visualized based on enhanced chemiluminescence. Proteins were quantified using ImageJ, and the levels were normalized to a control protein.

ELISA assay

Whole cell lysates prepared with RIPA buffer (Pierce) were cleared, and protein concentration was measured using BCA protein assay (Pierce). Around 10 μg total protein was analyzed using an ELISA kit (DLDLR0, R&D Systems) for human LDLR based on the manufacturer's protocol.

Prediction of 5′ UTR structures

Mfold (51) was used to predict the secondary structures of *RNASEH1*, *LDLR* and *ACP1* 5′ UTRs. RNAfold 2.1.8 (52) was used to predict secondary structures of the first 100 nucleotides of human and mouse mRNA transcripts; sequences were obtained from NCBI (53). Potential structured mRNA targets were identified as those with a predicted hairpin within the first eight nucleotides from the 5′ cap with at least 10 base pairs in the stem and folding energy less than –50 kcal/mol.

LDL uptake

HEK293 cells were treated with 30 nM ASOs for 15 h or with 5 nM control siRNA targeting *luciferase* or siRNA specific for *LDLR* mRNA for 4 h followed by ASO treatment for an additional 10 h. Medium was then changed to OPTI-MEM medium (Life Technologies) supplemented with 1% fatty acid free BSA (Sigma). After 1 h, bodipy-LDL (Life Technologies) was added at 5 μg/ml final concentration, and cells were incubated for 1 h. After three washes with 0.2 M glycine, 0.15 M NaCl (pH 3.0), cells were harvested and lysed using RIPA buffer. Internalized bodipy-LDL was quantified using a 96-well plate reader (Tecan) and normalized to total protein.

Pulse-chase labeling of nascent protein

HeLa cells were transfected with 60 nM ASO814923 for 7 h, and cells were labeled with ^{35}S-methionine as described previously (54). Cell lysates were prepared, and immunoprecipitation was performed using an anti-LDLR antibody (R&D, AF2148). Co-isolated proteins were separated by SDS-PAGE and transferred to a membrane. Labeled proteins were visualized by autoradiography.

Characterization of RNA-protein interactions

A 60-nucleotide fragment of the 5′ UTR of *ACP1* mRNA (XL745, see Supplementary Information) was synthesized and capped using vaccinia capping enzyme (New England BioLabs). Approximately 1 nM of capped RNA (XL745) was annealed with ∼1.2 nM ASO812658, control ASO XL398 or no ASO. The RNA/ASO samples were incubated for 45 min at 30°C with cell lysate containing ∼250 μg protein prepared from HEK293 cells, followed by addition of NaBH$_3$CN to a final concentration of 20 mM. After incubation at room temperature for an additional 30 min, the RNA-associated proteins were isolated using prewashed neutravidin beads by incubation at 4°C for 1 h. After extensive washing with wash buffer (20 mM HEPES, pH 7.5, 150 mM NaCl, 0.1% Tween and 0.2 unit/μl RNaseOut (Thermo-Fisher)), bound proteins were eluted using RNase One digestion, precipitated, and analyzed by western.

RNA immunoprecipitation

HEK293 cells were treated with 40 nM ASO targeting inhibitory region or a control ASO for 7 h, followed by UV-crosslinking. Cell lysates were prepared, and immunoprecipitation was performed using anti-eIF4A antibody (Abcam, ab31217) pre-coated on Protein A/G beads (Millipore). After incubation at 4°C for 2 h, beads were washed, and bound RNA was prepared using Trizol (Thermo-Fisher). Co-isolated RNAs were quantified by qRT-PCR. *ACP1* mRNA, *ACTB* mRNA, and 7SL RNA amounts were normalized to *DROSHA* mRNA.

RNA preparation and qRT-PCR

Total RNA was prepared from cells or liver homogenates using RNeasy (Qiagen). qRT-PCR was performed in triplicate as described previously (55) using TaqMan primer probe sets listed in the Supplementary Information in a StepOne Real-Time PCR system (Thermo-Fisher). Quantities were normalized to total RNA measured using SYBR Green (Thermo-Fisher). To detect splicing of *RNASEH1* pre-mRNA, reverse transcription was carried out using primers specific to *RNASEH1* (XL560) or *PTEN* mRNA. As a control, one set of reactions was performed without reverse transcriptase. PCR was performed for 25 cycles using primers XL295 and XL296 (for exons 1–2) or XL295 and XL560 (for exons 1–3) for *RNASEH1* mRNA or the primers for *PTEN* mRNA as used for qRT-PCR.

Subcellular fractionation

HEK293 cells grown in 15-cm dishes were transfected using Lipofectamine RNAiMax for 16 h with 25 nM *RNASEH1* ASO761919 or a control ASO761703. Cells were then harvested, and cytoplasmic and nuclear fractions were separated using PARIS kit (Thermo-Fisher) based on manufacturer's protocol. RNA was prepared from cytoplasmic and nuclear fractions using RNeasy (Qiagen). *RNASEH1*, *DROSHA*, and *Malat1* mRNAs were quantified using qRT-PCR.

RNA structural probing

Dimethyl sulfate modification and primer extension were performed as described (56). Briefly, HEK293 cells were treated (or not treated) with ASO813653 for 10 h and were incubated for 3 min at 37°C with 20 μl/ml dimethyl sulfate, followed by washing with ice-cold 30% β-mercaptoethanol. The cells were pelleted and washed with ice-cold PBS. Total RNA was prepared from cells using RNeasy (Qiagen).

Primer extension was performed with 7 μg total RNA using a primer XL505 labeled at the 5′ end with ^{32}P. The extension products were analyzed on an 8% polyacrylamide, 7 M urea gel next to DNA sequencing reactions performed using the same primer and a plasmid containing the 5′ UTR sequence of human *ACP1*.

In vivo study

Seven-week-old male BALB/c mice ($N = 3$) were given 25 or 50 mg/kg ASO827817 or ASO866017 (control) by subcutaneous injection. After 48 h, mice were given another injection of the same ASO at the same dose. Animals were sacrificed 48 h after the last dose, and liver homogenates were prepared and subjected to either western analysis for ACP1 protein or qRT-PCR analysis for *ACP1* mRNA. All tested animals were included in the analyses.

RESULTS

ASOs targeting a non-uORF region in the 5′ UTR of *RNASEH1* mRNA can increase the level of the encoded protein

Our recent finding that ASOs targeting uORF regions can enhance translation of the primary ORF promoted us to evaluate whether ASOs targeting other region within 5′ UTRs could also increase the amount of protein produced (29). We initially targeted the 5′ UTR of *RNASEH1*, which encodes the enzyme required for oligonucleotide-directed RNA cleavage. *RNASEH1* mRNA contains a uORF and we have found that ASOs that bind to the uORF start codon increase the amount of RNASEH1 produced (29,38). The secondary structure of the *RNASEH1* 5′ UTR predicted using Mfold (51) is shown in Figure 1A. We designed 16-nucleotide ASOs with phosphodiester backbones (PO) and 2′-*O*-methyl (Me) sugars to base pair with potential structured regions of the *RNASEH1* 5′ UTR. This type of ASO does not trigger cleavage of complementary RNA (57). Indeed, the level of *RNASEH1* mRNA was not significantly altered when these ASOs were transfected into HeLa cells (Supplementary Figure S1A).

The ASOs were transfected into HeLa cells, and RNASEH1 protein levels were determined by western analyses. Consistent with our previous findings (29), three ASOs targeting the uORF region (761909, 761915, 761916) increased the level of RNASEH1 protein (Figure 1B). Interestingly, treatment with ASO761919, which base pairs with region predicted to be part of a stem, increased the amount of protein to 214% of that in the mock-treated cells. Though ASO761918 modestly increased the protein level, ASO761917 did not have a significant effect on the quantity of RNASEH1, demonstrating that the effect on protein production is sequence dependent. The RNASEH1 protein produced in ASO761919-treated cells is functional, as in these cells but not in cells treated with a control ASO761703, we observed increased activity of a chimeric ASO designed to activate RNASEH1-mediated cleavage of *Malat1* RNA (Supplementary Figure S1B). These experiments and subsequent experiments were performed 3–5 times, and similar trends were observed, although the calculated protein levels varied somewhat due to the semi-

quantitative nature of western analyses. Representative results are shown for each experiment.

To determine if the ASO761919 target site in the 5′ UTR of *RNASEH1* mRNA is indeed inhibitory, mutations were made in this region and evaluated using a dual luciferase reporter system, in which the 5′ UTR of *RNASH1* mRNA was placed upstream of the firefly *luciferase* coding sequence (Supplementary Figure S2A). To eliminate the influence of the uORF, the uAUG was mutated to uUUG to inactivate uORF translation (H1m). This single mutation increased translation by approximately 7 fold (Supplementary Figure S2B and C), consistent with our previous observations (29). Within the uORF inactivated background, we found that mutation at the upstream sequence of the ASO targeted region (MT1), but not the downstream sequence (MT2), increased translation (Supplementary Figure S2B and C). Mutation at the opposite site of the predicted stem 1 (MT4) also increased translation, however, the compensatory mutation for this potential stem (MT5) did not restore inhibition. These results suggest that the site ASO761919 binds has an inhibitory effect on translation of *RNASEH1* mRNA. Since the compensatory mutation did not restore inhibition, the inhibitory effect may not be caused by the predicted stem structure. Other factors, such as protein binding or other secondary or higher order structures, may contribute to the inhibition effect, which is currently unclear and awaits further investigation (see discussion).

Effects of ASOs on the level of the protein were position dependent (Figure 1A and B). This position dependence was confirmed by analyses of ASOs targeting the ASO761919 region (Figure 1C). Treatment with these ASOs increased the protein level but to different extents (Figure 1D). To confirm that the ASO effect on the protein level depends on ASO/RNA hybridization, ASOs were designed to contain different numbers of mismatches to the target (Figure 1E). Increasing the number of mismatches significantly reduced the ability of the ASOs to increase the level of RNASEH1 protein (Figure 1F). In addition, co-transfection of ASO761919 with a complementary ASO (ASO927728), but not with a control ASO759704 (Figure 1G and H), diminished its effects on protein production without substantially altering *RNASEH1* mRNA levels (Figure 1I).

ASOs targeting the inhibitory region can enhance translation

Previously we found that ASOs targeting uORFs increase protein level through enhancing translation (29). We thus evaluated if this is also the case for ASOs targeting this non-uORF inhibitory region. As described above, transfection of the ASO761919 increased the protein level, but not the level of *RNASEH1* mRNA. This was confirmed in multiple experiments. As exemplified in Figure 2A, the *RNASEH1* mRNA levels were comparable in mock treated cells and in cells treated with ASO761919 or a control ASO761703, suggesting that the increased protein level was not a result of increased mRNA transcript. In addition, transfection of cells with ASO761919 did not substantially alter the subcellular distribution of *RNASEH1* mRNA. As controls, localization of *Drosha* mRNA and *Malat1* lncRNA, which are cyto-
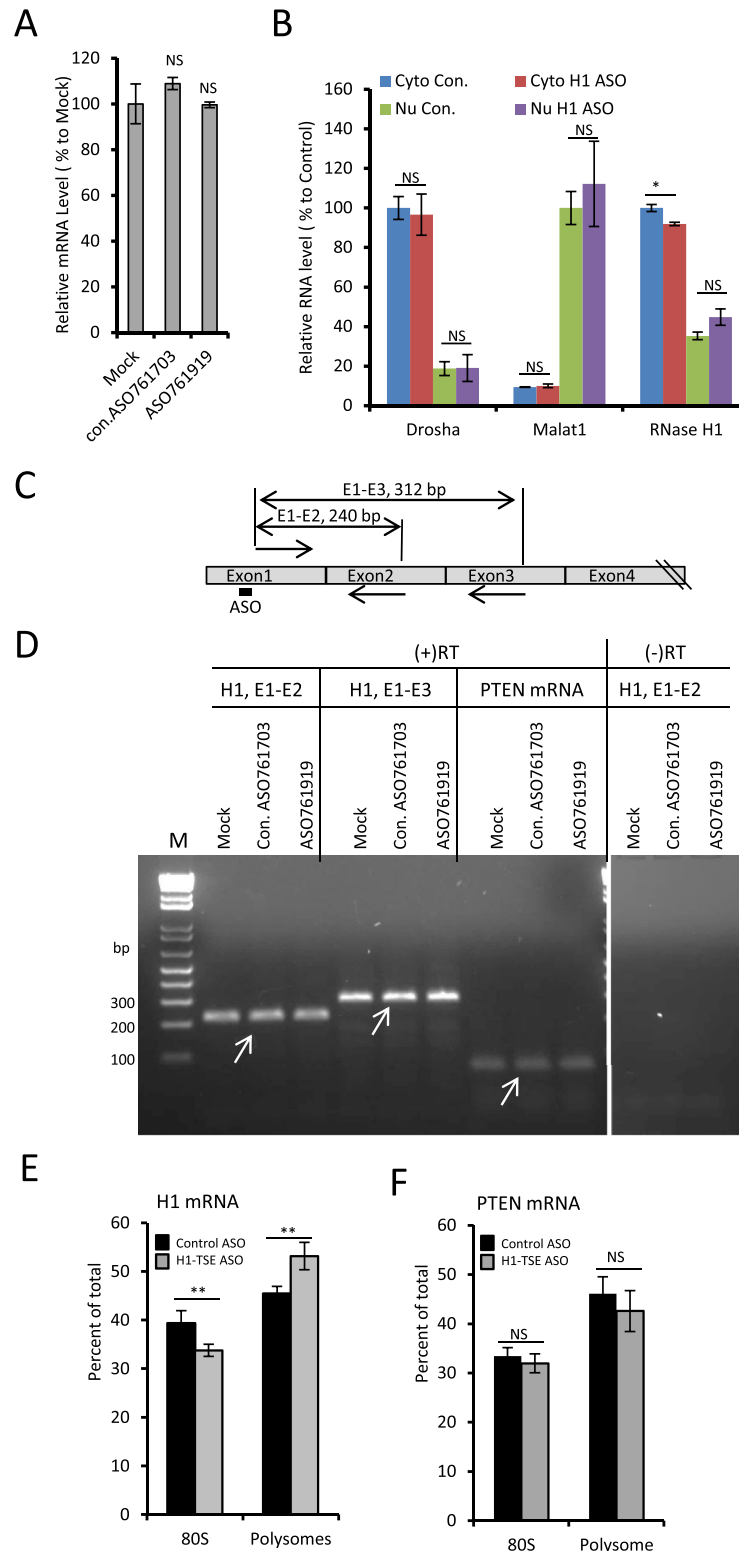
Figure 2. The ASO increases RNASEH1 protein level by enhancing translation. (**A**) qRT-PCR quantification of *RNASEH1* mRNA in HeLa cells treated with control ASO761703 or *RNASEH1* ASO761919 for 10 h. (**B**) qRT-PCR quantification of *DROSHA*, *Malat1*, and *RNASEH1* RNAs in cytoplasmic and nuclear fractions of HeLa cells treated with control ASO761703 or ASO761919 for 10 h. Plotted are mean relative RNA levels $\pm$ standard deviations of three experiments. (**C**) Schematic representation of the 5′ region of *RNASEH1* mRNA. Primers used for RT-PCR are indicated by arrows and the expected sizes of PCR products are shown. (**D**) The level and splicing patterns for exons 1, 2, and 3 of *RNASEH1* mRNA in ASO and control treated HeLa cells. *PTEN* mRNA served as a loading control. (**E**) qRT-PCR quantification of *RNASEH1* mRNA (left panel) or *PTEN* mRNA (right panel) in monosome (80S) and polysome fractions of HeLa cells treated with 30 nM ASO759704 (control) or ASO761919 for 7 h. The error bars are standard deviations from three experiments. *P*-values were calculated based on unpaired *t*-test. NS, not significant. *$P < 0.05$; **$P < 0.01$.

plasmic and nuclear RNAs (58), respectively, were analyzed (Figure 2B). In addition, the splicing pattern of *RNASEH1* pre-mRNA was not altered in ASO761919-treated cells compared to control ASO-treated cells, as shown by RT-PCR with primers designed to detect splicing of exons 1, 2 and 3, which are near the ASO binding site (Figure 2C-D). These data indicate that the increased protein level observed in cells treated with the ASO targeting the inhibitory region is not due to alteration of mRNA levels or isoforms.

Attempts to determine increased level of nascent RNASEH1 protein failed due to the low level of the protein and lack of highly specific, immunoprecipitation-grade antibody. To confirm that the ASO enhances translation of RNASEH1, polysome profile was analyzed using sucrose gradient fractionation, followed by qRT-PCR analyses for *RNASEH1* mRNA (Supplementary Figure S3). Transfection of the ASO761919 led to a shift of the *RNASEH1* mRNA toward polysome-containing fractions, suggesting enhanced translation of the mRNA. We note that this shift was modest but reproducible and was not observed when cells were treated with a control ASO. The distribution of *PTEN* mRNA in the gradient fractions was not significantly affected by ASO treatment.

To further confirm this observation, the gradient fractions containing 80S ribosome (fractions 9–13) and polysomes (fractions 15–25) were pooled, and RNA was prepared. qRT-PCR analysis showed that treatment with the ASO761919 increased the level of *RNASEH1* mRNA in polysome fractions accompanied by reduced levels in 80S fractions (Figure 2E, left panel). *PTEN* mRNA levels in monosome and polysome fractions were not affected by ASO treatment (Figure 2E, right panel). Together, these data suggest that ASO761919 enhances the translation of the targeted *RNASEH1* mRNA.

The ASO targeting the inhibitory region of *RNASEH1* 5′ UTR has minor off-target effects

The off-target effects of ASO are of concern (54). The ASO used here to target the inhibitory region in *RNASEH1* mRNA appears to have very minor non-specific effects on mRNA levels. ASO761919 has the potential to imperfectly base pair with several mRNAs including *CYTH3*, *PPP2R2C*, and *DMXL2* (Supplementary Figure S4A). The levels of these mRNAs were not affected by transfection of the ASO as determined by qRT-PCR (Supplementary Figure S4B). Importantly, CYTH3 protein levels were not affected by the ASO treatment (Supplementary Figure S4C). We attempted but failed to detect the other two proteins by western due to the low levels of expression in these cells. To further evaluate the effect of the ASO on gene expression at a global level, microarray analyses were performed. Genes that exhibited altered expression upon treatment with ASO761919 (absolute $\log_2$ ratio > 1, *P* value < 0.05) are listed in Supplementary Tables S1 and S2. Very minor changes in gene expression were observed: Modest increases were observed in 282 mRNAs and modest decreases were observed in 27 mRNAs in the ASO treated cells compared with mock treated cells. The number of affected genes is small, especially when compared with the effects of

siRNA transfection, which can cause altered expression of thousands of genes (59).

Changes in mRNA levels were modest with absolute $\log_2$ values <2. The basal expression levels of genes that showed altered expression upon the ASO treatment were generally low. The mean signal intensity of the entire gene population was ∼8500 units, whereas the means of the signal intensity for the increased or reduced genes were ∼2100 or 2400, respectively (data not shown). This low level of expression makes the level changes detected by microarray assay less reliable. To validate the altered expression of these genes, qRT-PCR was performed to detect the mRNA levels for five genes with increased signal in the microarray assay (*Abca2*, *FBP1*, *GPC5*, *PARK2* and *ACP1*), one gene with reduced signal (*CLCN5*), and one gene with no significant change (*DROSHA*) (Supplementary Figure S4D). No significant changes were detected, with the exception of *PARK2*. Levels of *PARK2* were increased by about 20% in the ASO treated cells. These results suggest that the changes in levels of mRNAs observed in microarray assay for many genes are false-positive signals, likely due to the low abundance of the mRNAs.

Consistent with the observation that the level of *ACP1* mRNA was not altered upon treatment of the *RNASEH1* ASO, the level of ACP1 protein was also not affected, as demonstrated by western analyses (Supplementary Figure S4E). Together, these observations suggest that the ASO has very minor off-target effects on the levels of mRNAs. The ASO appears to modulate translation in a manner dependent on both complementarity with target mRNA and the position of the base-pairing site in an mRNA, thus, in theory, the probability that such an ASO will modulate translation of a non-targeted mRNA is low.

As the ASOs can enhance translation without affecting the levels of mRNAs, it is possible that off-target effects are manifested as increased protein levels without alteration at the mRNA level. To evaluate this possibility, a proteomics study was performed to quantify protein levels in cells either mock-treated or treated with the ASO761919, using iTRAQ/TMT labeling followed by LC–MS/MS analysis, a method that has been used to detect protein level changes (60). Although RNASEH1 protein was not detected using this proteomics method, that RNASEH1 levels increased in the ASO treated sample was confirmed by western blot (Supplementary Figure S4F, inset). Of the 1990 proteins quantified by the mass spectrometry analysis (Supplementary Figure S4F and data not shown), none had significantly higher levels in the ASO-treated cells (based on an absolute $\log_2$ ratio greater than 1; *P* values were < 0.05) and only one (RRP44) was shown to be reduced (Supplementary Figure S4G). The mechanism for the reduction in RRP44 levels is unknown; the ASO had no significant base-pairing potential with this mRNA (data not shown). These results, together with the observations that the ASO modulates translation in both sequence and position dependent manner, suggest that the ASO has minor off-target effects.

LDLR mRNA contains an inhibitory structure in the 5′ UTR

To determine if ASOs can be used to increase the levels of other proteins, we analyzed the 5′ UTR of human *LDLR*

mRNA for potential secondary structures. The receptor encoded by this mRNA is required for cellular uptake and degradation of low-density lipoproteins (61). Agents that increase LDLR levels should reduce plasma cholesterol levels and thus have therapeutic potential (62). Although human *LDLR* mRNA contains two potential uORFs (Figure 3A and Supplementary Figure S5A), these uORFs probably have no or little effect on regulation of translation, as an AUG to UUG mutation of the first uORF did not have a significant effect on translation, as demonstrated using the dual luciferase reporter assay (Supplementary Figure S5B-C). Mutation of the second uORF caused only about a 40% increase in translation, which is very modest when compared with a known functional uORF. For example, mutation of the start codon at the *RNASEH1* uORF led to a 7-fold increase in translation activity (Supplementary Figure S2).

The 5′ UTR of *LDLR* mRNA is predicted to be highly structured, with a stem adjacent to the 5′ cap (Figure 3A). It has been well demonstrated that secondary structures in 5′ UTR can inhibit translation in a manner that is correlated with thermodynamic stability and is dependent on the proximity to the 5′ cap (40,42,44–48,63). Structures with more stable stems or shorter distance from the cap appear to be more inhibitory. This position-dependent effect was also confirmed in our study. We designed 18-mer ASOs modified with 2′-*O*-methoxyethyl to base pair with the 5′ UTR of *NCL1* mRNA to mimic potential duplex structures (Supplementary Figure S6A). The 5′ UTR sequence of *NCL1* mRNA near the cap is not predicted to contain secondary structure (data not shown). Consistent with previous findings (44,47,63), the ASO-mediated translation inhibition of the human *NCL1* mRNA occurred in a manner that was dependent on distance of the duplex structure from the cap (Supplementary Figure S6B). Though ASOs targeting positions beginning 6 to 12 nt from the cap reduced NCL1 protein levels, the inhibitory effect was significantly reduced when ASOs were hybridized further downstream (positions 14–18nt from the cap). We note that the ASOs targeting positions beginning 14 to 18 nt from the cap have slightly higher GC content (62.5%) than the ASOs targeting upstream sequences (56.25–62.5%) (Supplementary Figure S6C), suggesting that weaker inhibition was not due to lower binding affinity for the mRNA.

To determine if the predicted secondary structure of *LDLR* mRNA is inhibitory, mutational analyses were performed using the dual-luciferase reporter system. Complementary mutations were performed at either the 5′ or the 3′ side of the predicted stem structure to disrupt the potential base pairing or to generate compensatory mutations to restore the potential structure (Figure 3B). We found that mutations at either the 5′ or 3′ side of the predicted stem structure increased translation, with greater increase for the 3′ side mutation (Figure 3C). These data indicate that this region indeed suppresses translation of downstream pORF. Importantly, when compensatory mutation was performed, the inhibition effect was restored, supporting the view that the predicted structure, rather than the sequence, of the 5′ UTR of *LDLR* mRNA inhibits translation. The slightly enhanced inhibition may be explained by the observation that the original stem contains an A/C mismatch, whereas in the

compensatory mutation this was converted to U/G, which may lead to a more stable structure.

As the 5′ side mutation unexpectedly showed a weaker effect than the 3′ side mutation on translation inhibition in the reporter assay, we used Mfold to predict the structure formed with the mutant sequences. The 3′ side mutation was predicted to be less structured (data not shown); however, the sequence of the 5′ side mutation had the potential to form a 9-base-pair stem (Figure 3D) that involves position +2, which is closer to the 5′ cap than the original stem (+4) (Figure 3B). We then made mutants in which the 5′ (5d) or 3′ (3d) side of the stem was deleted (Figure 3E). The sequences after deletion were not predicted to form thermodynamically stable structures near the 5′ end of the 5′ UTR (data not shown). As a control, a region downstream from the stem was deleted (dd). Deletion of either the 5′ or the 3′ side of the potential stem led to an approximately 2-fold increase in the luciferase activity (Figure 3F), whereas the control deletion that does not affect the stem structure had no significant effect. Together, these results strongly suggest that the stem structure near the 5′ end of *LDLR* 5′ UTR inhibits translation.

ASOs targeting the structured region of *LDLR* increase LDLR protein levels

We designed ASOs with PO backbones and 2′-*O*-Me sugar modification to base pair with the 5′ or 3′ side of the predicted duplex in the *LDLR* 5′ UTR structure (Figures 3A and 4A). Since 5′ UTR structures can inhibit translation in a position-dependent manner (32,33,44), we reasoned that the ASO targeting the 3′ side of the stem should disrupt the hairpin near the 5′ cap, replacing it with a duplex formed with the ASO at a distance from the 5′ cap that should have little effect on translation, leading to increased protein levels (Figure 4A). On the other hand, we assumed that the ASO targeting the 5′ side of the stem structure, which will result in the formation of a perfect duplex between ASO and mRNA near the 5′ cap, would inhibit translation as effectively as the intramolecular mRNA secondary structure. Indeed, reduced levels of LDLR protein were observed when the 5′ side targeting ASO (XL824) was transfected into HEK293 cells, as determined by ELISA (Figure 4B). This result is consistent with our observations for the *NCL1*-targeted ASOs (Supplementary Figure S6) and with previous observations that structural elements have stronger inhibitory effects on translation when placed close to the 5′ cap (44,47). The reduced level of LDLR protein observed upon XL824 treatment was not due to decreased mRNA levels, since in cells treated with XL824 the level of *LDLR* mRNA was increased (Figure 4C), likely due to compensatory effects.

When cells were treated with the ASO targeting the 3′ side of the predicted stem (ASO814923), the level of LDLR protein was increased to ∼240% (Figure 4D). Other ASOs designed to hybridize near the binding site for ASO814923 also substantially increased the level of LDLR protein, although to different extents (Supplementary Figure S7A–C). When cells were treated with an ASO (XL506) targeting further downstream within the potential uORF region (Figure 3A), the levels of LDLR protein were comparable with the
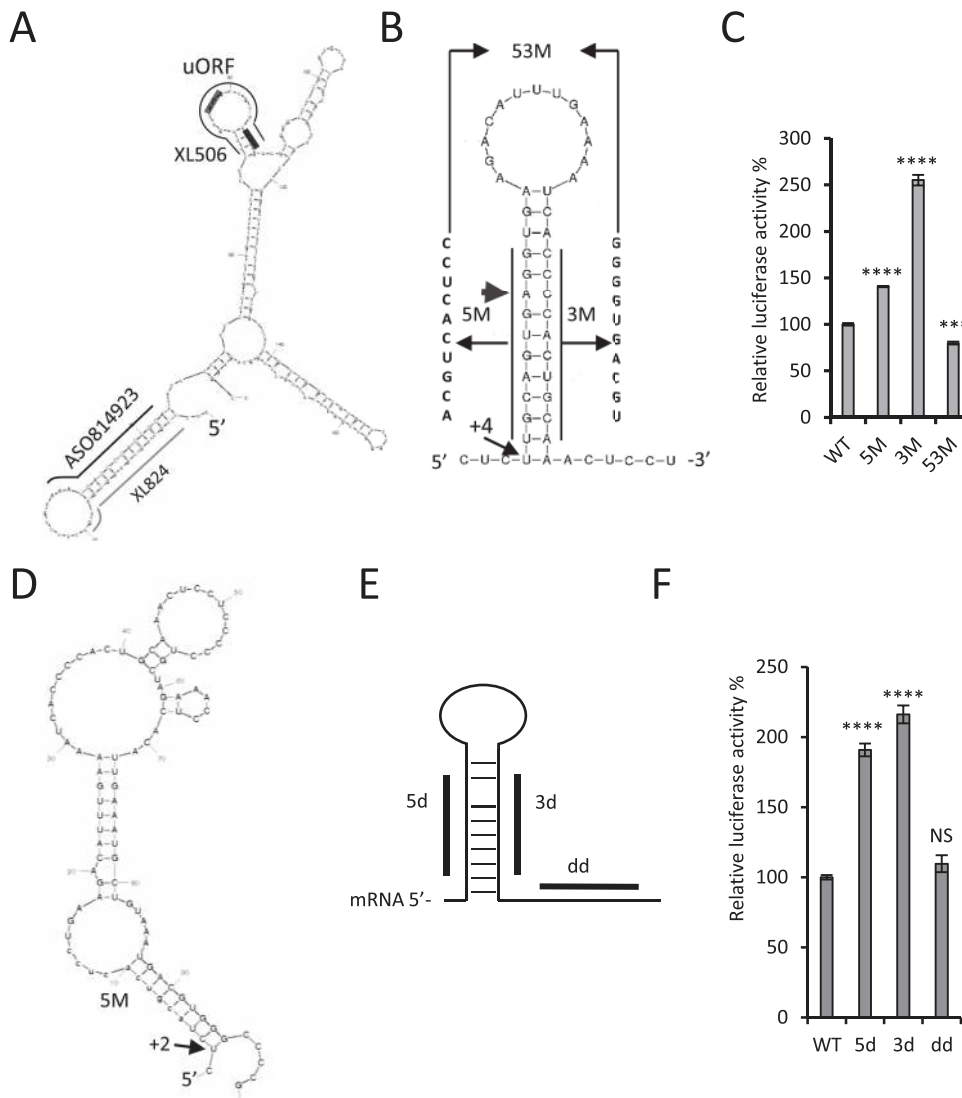
Figure 3. Predicted structure in *LDLR* 5′ UTR inhibits translation. (**A**) Predicted secondary structure of a region of the 5′ UTR of human *LDLR* mRNA. The shadowed areas indicate uAUGs. The ASO binding sites are indicate by lines. (**B**) RNA sequence and mutations in the predicted structure region of *LDLR* mRNA; sequence is shown for the region of the mRNA beginning at position 1. The stem structure involves the base at position +4. The complementary mutations are indicated. The arrow head indicates an A–C mismatch. (**C**) Luciferase activity of the reporters containing wild-type or mutated *LDLR* 5′ UTR sequences shown in panel B analyzed in HEK293 cells. (**D**) Predicted secondary structure of the *LDLR* 5′ UTR with the 5′ side mutation. The position of newly formed stem structure relative to the 5′ end is indicated; this stem involves the base at position +2. (**E**) Schematic of structure and deletion mutations in the predicted structure region of *LDLR* 5′ UTR. (**F**) Luciferase activity of the reporters containing deletions shown in panel E. Error bars are standard deviations of three experiments. *P* values were calculated based on unpaired *t*-test. NS, not significant. ***$P < 0.001$; ****$P < 0.0001$.

levels in mock-treated cells (Figure 4D). This result is consistent with observations from our mutational analysis that indicate that the uORF of *LDLR* mRNA is not highly inhibitory (Supplementary Figure S5).

ASOs targeting the inhibitory structure enhance translation efficiency of LDLR and increased the LDL uptake

That the ASO treatment increased the level of LDLR protein was also confirmed by western analysis (Figure 4E). The ASO814923 targeting the 3′ side of the inhibitory structure did not alter the *LDLR* mRNA levels as shown by qRT-PCR (Figure 4F), consistent with the hypothesis that the ASO enhances translation. To confirm this, pulse-chase labeling was performed using ^{35}S-methionine, followed by immunoprecipitation with an antibody to LDLR protein. As shown in Figure 4G, the level of nascent LDLR protein was significantly increased in the ASO treated cells, to ∼310% relative to mock-treated cells (Figure 4G, left panel). Polysome profile analyses also indicate that ASO814923 enhances translation. While the migration profiles of 28S rRNA were superimposable for control or the ASO treated cells (Supplementary Figure S8A and D), *LDLR* mRNA was modestly shifted toward polysome regions in cells treated with this ASO (Supplementary Figure S8B), suggesting increased translation. As a control, the ASO targeting the 5′ side of the stem that reduced LDLR
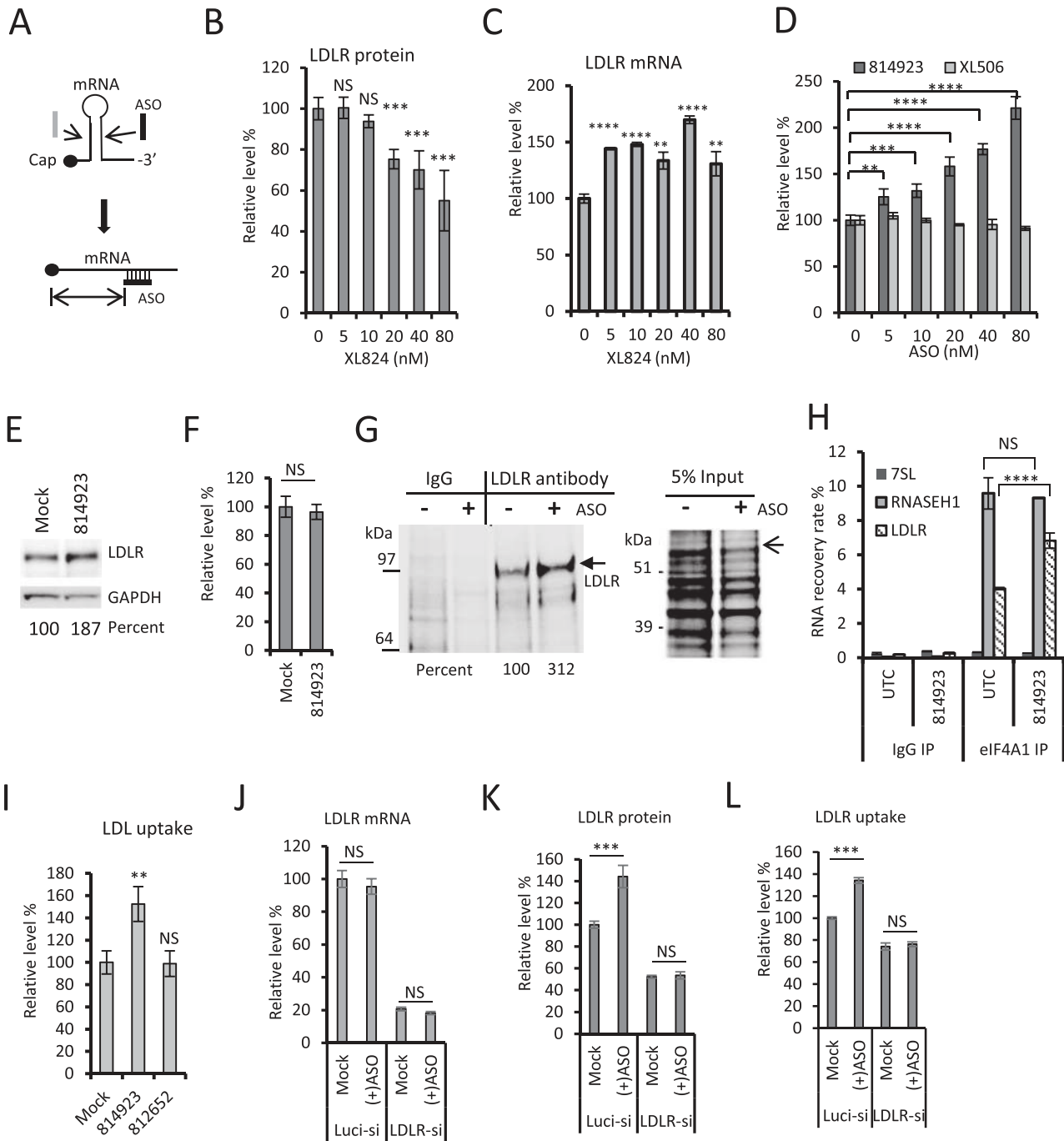
Figure 4. Translation of LDLR protein is enhanced by targeting the predicted structure using an ASO. (**A**) The potential effect of an ASO on the predicted structure is depicted. (**B**) ELISA analyses for LDLR protein levels in HEK293 cells transfected for 15 h with XL824, which targets the 5′ side of the predicted stem. (**C**) qRT-PCR quantification of *LDLR* mRNA in cells treated with XL824. (**D**) ELISA analyses for LDLR protein in HEK293 cells transfected for 15 h with ASO814923, targeting the 3′ side of the potential stem or an ASO XL506 targeting a potential uORF. ASO concentration 0 indicates mock transfection. (**E**) Western analyses for LDLR protein in HEK293 cells treated with 30 nM ASO814923 for 10 h. Levels were normalized to those of GAPDH. (**F**) qRT-PCR quantification of *LDLR* mRNA levels in HEK293 cells treated with the ASO. (**G**) Autoradiography of ^{35}S-methionine-labeled nascent LDLR protein isolated by immunoprecipitation from cells treated with ASO814923 (+) or mock-treated (–) for 7 h. An aliquot of cell lysate used for immunoprecipitation was analyzed by SDS-PAGE, and labeled nascent proteins were visualized by autoradiography (right panel). The level of nascent LDLR protein was normalized to signal from band marked by an arrow, and relative levels are given below the lanes. (**H**) qRT-PCR quantification of *LDLR* mRNA co-immunoprecipitated using an anti-eIF4A antibody or control IgG from mock transfected HEK293 cells (UTC) or cells treated with the ASO814923 for 10 h. 7SL RNA and *RNASEH1* mRNA were quantified as controls. (**I**) LDL uptake in HEK293 cells treated with 30 nM ASO814923 or 30 nM control ASO812662 for 15 h. (**J**) qRT-PCR for *LDLR* mRNA levels in HEK293 cells treated with siRNA targeting *luc* or *LDLR* for 4 h, followed by treatment with or without ASO814923 (40 nM) for an additional 10 h. (**K**) ELISA analyses for LDLR protein levels in HEK293 cells treated with siRNAs, followed by treatment with ASO814923. (**L**) LDL uptake in HEK293 cells treated with siRNAs for 4 h, followed by treatment of the ASO for 10 h, and LDL uptake analysis. The error bars are standard deviations from three experiments. *P*-values were calculated based on unpaired t-test. NS, not significant. ***P* < 0.01; ****P* < 0.001 and *****P* < 0.0001.

protein level caused shift of the *LDLR* mRNA toward the top of the gradient (Supplementary Figure S8E), indicating a reduction in translation. The ASOs were specific for the targeted *LDLR* mRNA as the migration patterns of an untargeted *PTEN* mRNA were not substantially altered by either ASO (Supplementary Figure S8C and F).

To further confirm an enhanced translation of *LDLR* mRNA by the ASO814923, immunoprecipitation was performed using an antibody against translation factor eIF4A1. Upon treatment with the ASO, significantly more *LDLR* mRNA was precipitated with eIF4A1, as compared with that from control cells. *RNASEH1* mRNA was recovered to a similar extent from treated and untreated cells, but little 7SL RNA, a non-coding RNA, was precipitated with eIF4A1 (Figure 4H). Together, these results indicate that the ASO enhanced translation efficiency of *LDLR* mRNA.

LDLR mediates cellular uptake of LDL from plasma *in vivo* (61). For patients with high levels of cholesterol, it is therapeutically beneficial to increase LDLR protein levels as thus enhances the clearance of the LDL-cholesterol. To determine if the ASO that increases the level of LDLR protein also promotes LDL uptake, cells pre-treated with the ASO were incubated with bodipy-labeled LDL for 1 h. The level of internalized LDL was then measured. LDL uptake was increased by approximately 50% in cells treated with this ASO, compared with mock treated cells and with cells treated with a control ASO812652 (Figure 4I). In addition, it appears that the ASO-mediated increase of LDL uptake is dependent on the level of LDLR protein, as reduction of the *LDLR* mRNA using siRNA treatment abolished the ASO effect (Figure 4J–L). This result indicates that the protein produced from the *LDLR* mRNA targeted by the ASO is functional and that ASO treatment can lead to phenotypical changes related to the biological function of the protein encoded by the targeted mRNA.

Chemical modifications enhance the ASO activity

ASO814923 is a 2′-*O*-Me ASO linked with PO backbones. ASOs that are active *in vivo* must be chemically modified to ensure stability in serum and to facilitate delivery into tissues. We therefore synthesized ASO842196, which has the same sequence and 2′-*O*-Me modifications as ASO814923 but has a phosphorothioate (PS) backbone. Compared with PO-ASOs, PS-ASOs exhibit dramatically enhanced pharmacological properties (64). PS-ASOs dosed systemically distribute to different organs (65). The PS-ASO (ASO842196) was transfected into HeLa cells, and the level of LDLR protein was determined by ELISA. The results showed that ASO842196 treatment significantly increased the protein level, to ∼2.5-fold of that in mock treated cells (Figure 5A). Similarly, the PS-ASO (ASO842196) also increased the LDLR protein level in HEK293 cells (Figure 5B). These results indicate that the PS-backbone ASOs targeting 5′ UTR inhibitory structure can increase protein levels in different cell types.

In our studies on the effects of ASOs on uORF-mediated translation, we demonstrated that there is a balance between the ability of the ASOs to bind to the uORF region and the requirement that the ASO must be removed in order for the ribosome to translate the mRNA (29). Un-
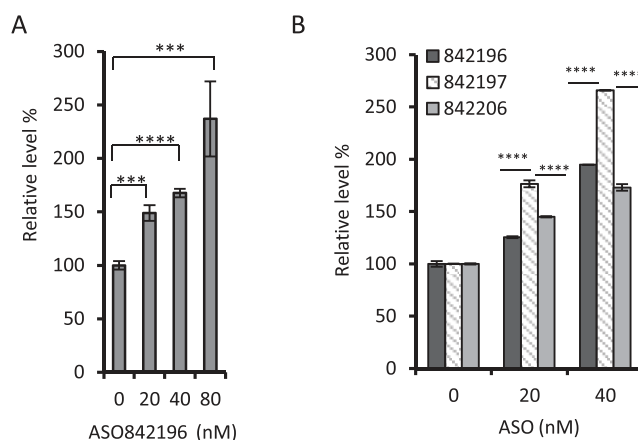
Figure 5. ASOs with different modifications can increase LDLR protein levels. (**A**) ELISA analysis for LDLR protein levels in HeLa cells treated with ASO842196 for 15 h at different concentrations. (**B**) ELISA analyses for LDLR protein levels in HEK293 cells transfected with ASO842196, ASO842197, or ASO842206 at indicated concentrations for 12 h. Means ± standard deviations of three independent experiments are plotted. *P*-values were calculated based on unpaired *t*-test. ***$P < 0.001$; ****$P < 0.0001$.

like uORFs, which decrease pORF translation efficiency by causing initiation at an inappropriate AUG, 5′ UTR structures can inhibit PIC binding or scanning along the 5′ UTR, in a position and thermodynamic stability dependent manner (29,33,44,47,63). To analyze the role of affinity of the ASO targeting the inhibitory structures, we synthesized ASOs with the 2′-constrained-ethyl (cEt) modification, which increases the thermal stability of the duplex by 3.5–4.5°C per modification (66). The 16-mer, cEt-modified ASO842197 was more potent than the PS/Me-ASO (ASO842196), with an increase in LDLR protein level to 270% (Figure 5B), likely because the higher affinity of the cEt-containing ASO allows it to invade the secondary structure more effectively than does the PS/Me-ASO. However, when the affinity was further increased using an 18-mer cEt-containing ASO (ASO842206), the activity was reduced compared with the 16-mer cEt-containing ASO, suggesting that there is an optimal affinity for ASOs targeting the inhibitory structures.

Identification of potential secondary structures and targeting of such structure in *ACP1* mRNA

In addition to *LDLR*, translation inhibition by 5′ UTR secondary structure has been observed in different mRNAs in different eukaryotic cells, such as *CYC1*, *HIS4*, *PYK1*, *PDGF* and *ODC* mRNAs (67–71). To enable broader application of ASOs targeting structural inhibitory elements in other mRNAs, we developed an *in silico* approach to predict potential structures. It has been shown previously that among the many factors that may affect translation, the 5′ UTR secondary structure (free energy) is the most predictive variable, followed by other factors including uORFs and the presence of stable secondary structures within the first 100 nt from the cap (34). Thus, secondary structures were predicted for the first 100 nucleotides of 5′ UTRs of all available human and mouse mRNAs, and free en-

ergies were calculated for the potential stem structures as described in the Materials and Methods section. The mRNAs were sorted based on free energy; ∼56% of human and mouse mRNAs were predicted to contain potential secondary structures with free energies less than –30 kcal/mol (data not shown). The 25 mRNAs that potentially form the lowest free energy structures are listed in Supplementary Table S3.

Among these mRNAs, human *ACP1* mRNA was selected for further study due to the abundance of the protein in cells and the availability of antibodies. In addition, this mRNA does not contain a potential uAUG (data not shown). ASOs were designed to target a predicted hairpin near the 5′ cap and a downstream stem structure (Figure 6A). Treatment of HEK293 cells with 16-mer 2′-*O*-Me-modified ASOs with either PO (ASO812653) or PS (ASO812675) backbones targeting the 3′ side of the 5′-most stem structure dose-dependently increased the level of ACP1 protein (Figure 6B and C). Increased protein levels were also achieved with an 18-mer PS-ASO modified with both 2′-*O*-Me and cEt (ASO813860) targeting the same region (Figure 6D). A 16-mer PO/2′-*O*-Me-modified ASO (ASO812652) targeting a region slightly downstream also increased the protein level (Figure 6E), but to a lesser extent than ASO812653, again indicative of a positional effect. Indeed, ASO812655, which targets a downstream stem, had no effect on the level of ACP1 protein (Figure 6F). This hairpin is not in close proximity to the 5′ cap and probably does not act to inhibit translation, like previously demonstrated for the positional effects (44). Consistent with the observations made during our analysis of ASOs targeting *LDLR* mRNA (Figure 3C), an ASO targeting the 5′ side of the predicted stem near the cap of *ACP1* mRNA reduced the ACP1 protein level (Figure 6G), without reducing the levels of *ACP1* mRNA (Figure 6H), again consistent with previous observations of a distance-dependent effect of the 5′ UTR structures on translation (33).

ASOs targeting the potential 5′ UTR structure of *ACP1* mRNA enhances the recruitment of translation initiation factors

The *ACP1* mRNA contains a potential secondary structure but not a uORF. We thus used this mRNA as a model target to study the potential mechanism of how ASOs targeting the potential structured region enhance translation. Consistent with observations described above for *RNASEH1* and *LDLR* ASOs, ASO812653 treatment did not substantially alter *ACP1* mRNA levels (Supplementary Figure S9A). Although an 18-mer PO/Me ASO targeting the potential structure region increased ACP1 protein levels (Supplementary Figure S9B), a mismatched ASO targeting the same site did not (Supplementary Figure S9C and D).

Translation of ACP1, as well as LDLR, appears to be cap-dependent, since treatment of cells with 4E1Rcat, a small molecule that inhibits cap-dependent translation by disrupting the interaction between eIF4E and eIF4G, reduced ACP1 protein production (Figure 7A). In our study of uORF-targeted ASOs we showed that helicases known to be involved in translation, such as DHX29 (72), is required for the ASO-mediated translation activation (29). The effect

of the *ACP1* targeted ASO was also dependent on the helicases, since in cells depleted of DHX29 using siRNA, the ASO did not enhance translation as it did in control cells treated with luciferase siRNA (Figure 7B and C). These observations imply that the ASO targeting the predicted structure needs to be removed from the mRNA by helicases during scanning by the PIC, and that the mRNA structure may thus be dynamic, as described previously (73). Consistent with this view, dimethyl sulfate modification patterns in the 5′ UTR of *ACP1* mRNA were similar in the presence and absence of the ASO (Supplementary Figure S9E).

To confirm that the predicted secondary structure in the 5′ UTR of *ACP1* mRNA is indeed inhibitory, mutational analyses were performed in a dual luciferase reporter system (Supplementary Figure S10A). Mutation of either the 5′ or the 3′ side of the predicted stem significantly increased translation efficiency (Supplementary Figure S10B), indicating that this region is inhibitory. Interestingly, the compensatory mutation did not fully restore the inhibitory effect to wild-type levels (Supplementary Figure S10B). This observation suggests that other factors, such as protein binding or higher order structure, may also contribute to the inhibition by this region.

To evaluate whether the ASO targeting the inhibitory region of *ACP1* mRNA affects the loading of translational machinery to the mRNA, affinity selection from cell lysate was performed using a synthetic 5′-capped and 3′-biotinylated RNA derived from the *ACP1* mRNA 5′ UTR sequence. This RNA was annealed with ASO812658 that base-pairs with the 3′ side of the predicted stem or was incubated with a control ASO prior to affinity selection. The selected proteins were eluted by RNase treatment and analyzed by western blotting. A substantial increase in the binding of eIF4A and eIF2a proteins to the RNA was observed in the presence of ASO812658, compared with a control ASO or no ASO (Figure 7D). This suggests that the binding of ASO812658 enhances the recruitment of PIC. Consistent with increased binding of initiation factors to *ACP1* mRNA upon the ASO binding, slightly more *ACP1* mRNA was co-isolated with eIF4A from cells treated with ASO812658 compared with that from cells treated with a control ASO (Figure 7E, left panel). The non-coding 7SL RNA was not co-purified with eIF4A with either ASO (Figure 7E, middle panel). Further, *ACTB* mRNA, which has a similar length of 5′ UTR as the *ACP1* mRNA, was comparably recovered from untreated and ASO treated cells (Figure 7E, right panel), similar to what was observed for the ASO targeting the 5′ UTR inhibitory structure of *LDLR* mRNA (Figure 4H). Together, these results suggest that the ASO targeting the 3′ side of the inhibitory stem region enhances recruitment of translation initiation factors to the target mRNA.

An ASO targeting the inhibitory structure increases the level of ACP1 protein in mouse cells and in mice

Next, we evaluated whether the predicted structures in human are also present in mouse mRNAs. No significant structures were found near the 5′ cap for mouse *LDLR* mRNA, and ASOs targeting the 5′ UTR of mouse *LDLR* did not significantly increase the level of the protein in mouse MHT cells (data not shown). This suggests that regu-
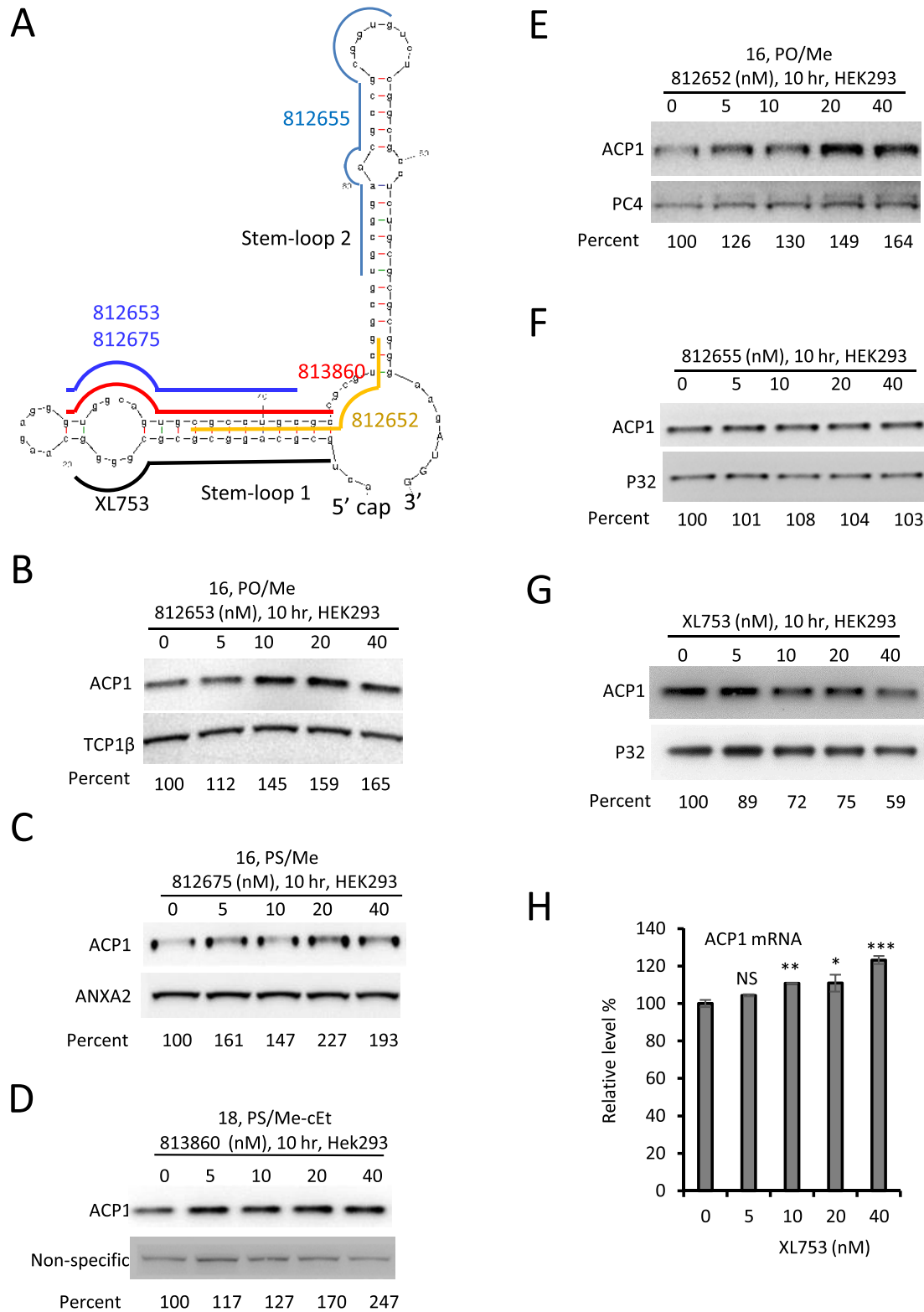
Figure 6. ASOs targeting a predicted stem structure in the *ACP1* 5′ UTR increase ACP1 protein levels in HEK293 cells. (**A**) The predicted secondary structure of a region of the 5′ UTR of human *ACP1* mRNA. The ASO binding sites are indicated by lines. The upper case letters in the mRNA indicate coding region sequence. Western analyses were performed to detect ACP1 protein in HEK293 cells transfected for 10–15 h with a 16-mer PO/Me ASO (**B**) and a PS/Me ASO (**C**), an 18-mer PS/Me-cEt ASO (**D**), a 16-mer PO/Me ASO targeting a slightly downstream sequence (**E**), and an 18-mer PO/Me ASO targeting a further downstream stem (**F**). A 16-mer PO/Me ASO targeting the 5′ side the 5′-most stem was also tested (**G**). Proteins used as loading controls are indicated in each panel. The percentages of ACP1 relative to protein levels in mock treated cells are listed below the lanes. (**H**) qRT-PCR for the levels of *ACP1* mRNA in cells treated with XL753 for 10 h. Means ± standard deviations of three independent experiments are plotted. *P*-values were calculated based on unpaired *t*-test. **$P < 0.01$.
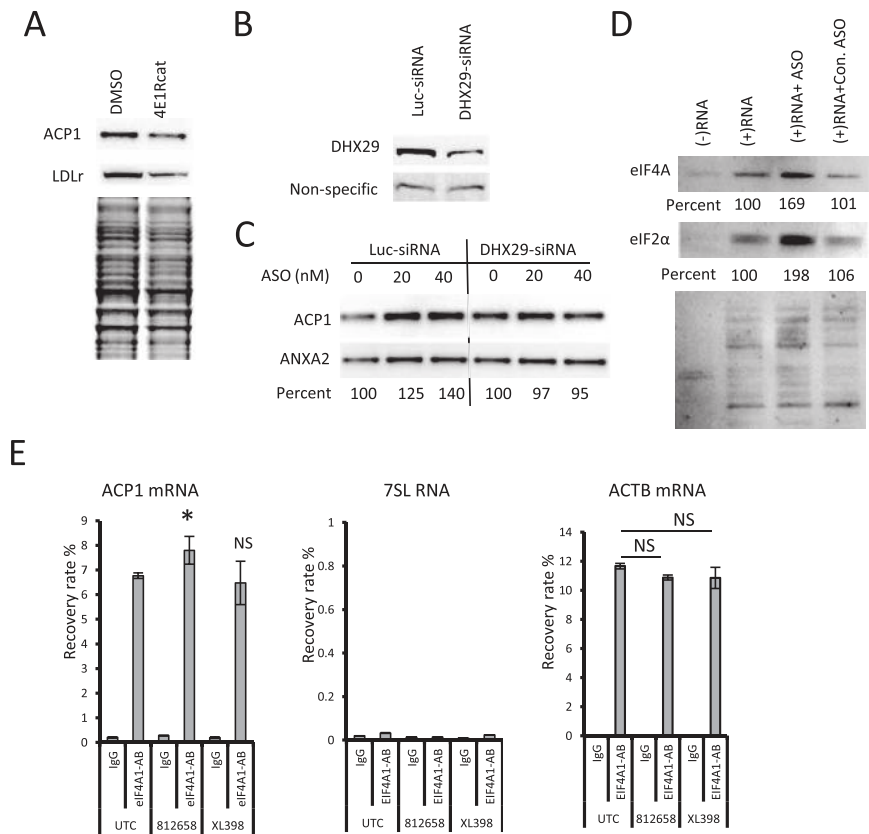
**Figure 7.** The *ACP1* ASO enhances binding of translation initiation factors to *ACP1* mRNA. (**A**) Western analyses of ACP1 and LDLR proteins in HeLa cells treated for 30 h with 15 μM 4E1Rcat. The lower panel shows a Coomassie-blue stained image from a duplicate gel, which serves as control to ensure equal loading. (**B**) Western analysis for DHX29 in HEK293 cells treated with 3 nM siRNAs targeting *DHX29* or *luc* for 24 h. (**C**) Western analysis for ACP1 protein in HEK293 cells treated with *DHX29* or *luc* siRNAs for 24 h, followed by transfection of ASO812653 for an additional 10 h. ANXA2 served as a loading control. The percentages of ACP1 protein relative to mock treated cells (ASO concentration 0) are shown below the lanes. (**D**) Western analyses for eIF4A (upper panel) and eIF2a (middle panel) proteins co-isolated with a 3′-biotinylated, 5′-capped RNA derived from the 5′ UTR of human *ACP1* mRNA in the presence of ASO812658, control ASO XL398, or no ASO. The same membrane was re-probed using rabbit serum to detect non-specific band that served as loading control (lower panel, indicated by an asterisk). Percentages relative to samples with no ASO are given. (**E**) qRT-PCR quantification of *ACP1* mRNA (left panel), 7SL RNA (middle panel), and *ACTB* mRNA (right panel) co-immunoprecipitated using an anti-eIF4A antibody or a control IgG from cells transfected with indicated ASOs or mock-transfected cells (UTC). Plotted are means ± standard deviations from three experiments. *P*-values were calculated based on unpaired *t*-test. NS, not significant. *$P < 0.05$.

lation of *LDLR* translation is different in human and mouse cells. A stem structure is predicted to form near the 5′ end of the mouse *ACP1* mRNA (Figure 8A), and the mRNA sequence in this region is conserved between human and mouse (not shown), suggesting that translation of mouse *ACP1* mRNA may be similarly regulated like the human mRNA. PO and PS ASOs with 2′-*O*-Me sugars were designed to target the 3′ side of the predicted stem of mouse *ACP1* mRNA (Figure 8A). Transfection of mouse MHT cells with ASOs targeting the stem significantly increased the level of ACP1 protein relative to levels in mock treated cells (Figure 8B and C). These data suggest that the 5′ UTR mediated regulation of *ACP1* mRNA translation is conserved between human and mouse, and that ASOs targeting the potential inhibitory region can increase the protein level in mouse cells. That 5′ UTR inhibitory structures are targetable with ASO in mouse cells was further demonstrated by experiments that showed that an ASO targeting the 3′ side of a predicted 5′ UTR stem structure of the mouse

ARF1 mRNA increased the level of ARF1 protein in MHT cells (Supplementary Figure S11).

We next investigated whether an ASO targeting a 5′ UTR inhibitory region could increase the level of protein in mice. For this experiment, a version of the ASO targeting the *ACP1* mRNA with a PS backbone was synthesized to ensure delivery *in vivo*. This ASO (ASO827817) or a control (ASO866017) was injected subcutaneously into mice ($N = 3$) at 25 or 50 mg/kg; dosing was repeated 48 h later. Mice were sacrificed 48 h after the last dose, and liver samples were prepared. Western analyses showed that the ACP1 protein was increased by 58% ($P = 0.027$, 95% confidence interval (CI) 10.7–105.2%) and 67% ($P = 0.007$, 95% CI 30.4–103.8%) in mice treated with 25 and 50 mg/kg ASO827817, respectively, compared with ACP1 protein levels in mice treated with saline, whereas the control ASO did not have a significant effect (Figure 8D–F). Consistent with the *in vitro* observations, the *ACP1* mRNA levels were comparable in control ASO- or *ACP1* ASO-treated mice (Figure 8G).
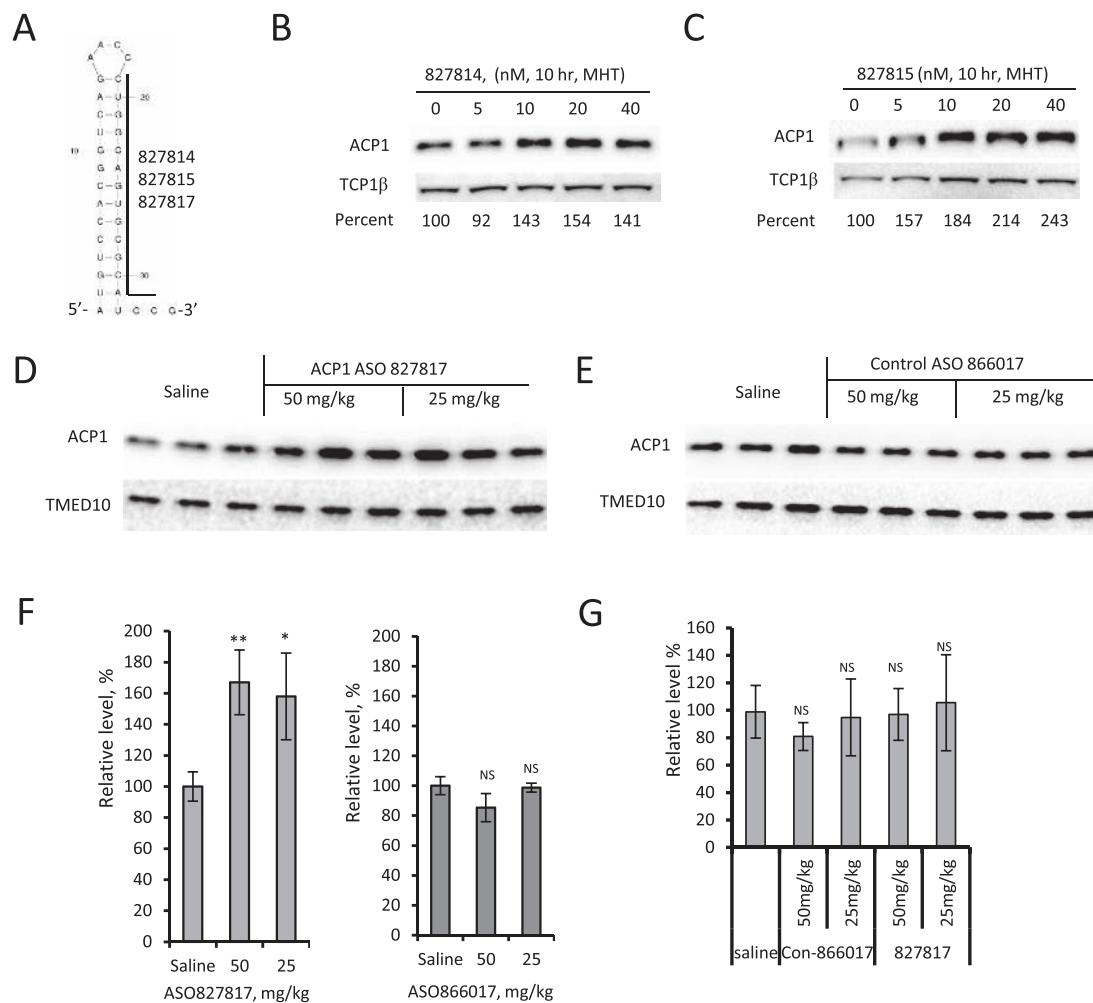
Figure 8. ASO treatment increases ACP1 protein levels in mouse cells and in animals. (**A**) The predicted secondary structure of a region of the 5′ UTR of mouse *ACP1* mRNA. The binding site for the ASOs is indicated. (**B**) Western analysis for ACP1 in MHT cells transfected for 10 h with PO ASO827814. TCP1β served as a loading control. (**C**) Western analysis for ACP1 in MHT cells transfected for 10 h with PS ASO827815. TCP1β served as a loading control. Percentages relative to mock treated samples are given. (**D**) Western analyses for ACP1 protein levels in liver homogenates of mice (N = 3) treated twice at a 48-h interval with *ACP1* ASO827817. (**E**) Western analysis for ACP1 protein levels in liver homogenates of mice treated with control ASO866017. TMED10 served as a loading control. (**F**) Quantification of ACP1 as a percentage of protein in saline-treated mice. Error bars represent standard deviations (*N* = 3). *P*-values were calculated based on unpaired *t*-test. *P < 0.05; **P < 0.01; NS, not significant. (**G**) qRT-PCR quantification of *ACP1* mRNA levels in the liver samples from mice treated with different ASOs. Equal portions of liver homogenates from each group were pooled, and total RNA was prepared and subjected to qRT-PCR. The error bars represent standard deviations from three independent experiments.

DISCUSSION

An approach that would enable an increase in levels of a specific protein *in vivo* would be therapeutically useful. Several approaches have been developed for this purpose including virus-mediated delivery of DNA constructs, formulated delivery of mRNAs, and inhibition of repression elements (8,74). Challenges in delivery and other issues limit broad utilization. Previously we reported that ASOs targeting uORFs of mRNAs can specifically increase the levels of targeted proteins (29), but not all mRNAs contain uORFs and some uORF may not be inhibitory. Here we used ASOs to disrupt other inhibitory elements in the 5′ UTRs. By targeting predicted inhibitory structures, we showed that three human proteins (RNASHE1, LDLR and ACP1) and two mouse proteins (ACP1 and ARF1) could be increased using ASOs. Importantly, protein levels were increased in mice by subcutaneous injection of chemically modified ASOs without the need of formulation.

Many factors, including mRNA structure, protein binding, and miRNA binding, can inhibit translation. Disruption of these inhibitory elements using *trans*-acting ASOs may thus lessen the suppression effects, leading to increased translation efficiency and higher protein levels. Translation regulation by 5′ UTRs is not fully understood, however, the inhibitory effect of uORFs and 5′ UTR structures has been well demonstrated (19,27,33,75). Some mRNA 5′ UTRs, including those listed in the Supplemental Table S3, are GC rich and might form G-quadruplex or other higher order structures that could be targeted with ASOs (37). Some predicted structural elements, such as the one present in the 5′ UTR of *RNASHE1* mRNA, are not G rich and the predicted secondary structure does not have high thermodynamic stability. The ASO targeting region in *RNASEH1* 5′

UTR is inhibitory, yet the compensatory mutation for the predicted stem structure did not restore inhibition. It is currently unclear how this region inhibits translation. It is possible that this region may form a different secondary structure, or a higher order structure, or may interact with *trans*-acting factors to inhibit translation. Translation inhibition by 5′ UTR elements other than the structural inhibitory elements is less well-understood, and likely to be mRNA specific. Indeed, it has been reported that *CFTR* mRNA contains an inhibitory element that does not have the potential to form strong secondary structures (36). Further detailed studies are required to better understand additional mechanisms by which translation is regulated. This will be important both for understanding translation and for using ASOs and other approaches to modulate these mechanisms. Nevertheless, for some mRNAs without predictable secondary structures, it might still be possible to increase protein levels by screening with ASOs that target regions throughout the 5′ UTR.

Although computational prediction of 5′ UTR secondary structures may yield false positive results, *in silico* prediction can help to narrow down the potential target sites. Targeting the predicted secondary structures for *LDLR*, *ACP1*, and *ARF1* mRNAs specifically increased the protein levels more than 2 fold. Mutational analyses for the *LDLR* mRNA demonstrated that the predicted stem structure, but not the sequence of this region of the 5′ UTR, is inhibitory, consistent with previous observations for 5′ UTR structural effects (76). The inhibitory effect of the predicted structural region of the *ACP1* mRNA was also confirmed through mutational analysis. It appears that the predicted secondary structure is only partially inhibitory, as shown by analysis of the compensatory mutation (Supplementary Figure S10). Other factors, such as higher order structure or protein binding, must also contribute to the inhibitory effect.

Previous studies have shown that strong stem structures near the cap can inhibit translation in a position-dependent manner (44,47). When the stem was placed further from the cap, the inhibitory effect was reduced. Similarly, we found that ASOs that base pair with the 5′ UTR of *NCL1* mRNA, thus mimicking duplex structures, also showed position-dependent inhibitory effect. Importantly, ASOs targeting the 3′ side of the predicted stem structures of 5′ UTR increased protein levels; however, ASOs targeting the 5′ side of the predicted stems of *LDLR* and *ACP1* mRNAs led to reduced levels of proteins and reduced translation, as evidenced by the results of polysome profile analysis for *LDLR* mRNA. These results further support a positional effect of potential structures on translation, as demonstrated previously (33). Thus, it is likely that ASOs targeting the 3′ side of a stem structure near the 5′ cap alter the favored intramolecular stem structure and increase the distance from the cap to the duplex region, leading to increased translation efficiency. However, we note that the ASOs might also produce effects through other elements in the 5′ UTR, such as downstream potential uORFs (for the case of RNASEH1 and LDLR), although translation initiation in the 5′ UTR of human *LDLR* mRNA was not identified in a recent study focused on identifying translation initiation sites at a global level (31).

The increase in protein levels by ASOs, though modest, appears to be specific to the target gene. The increase in protein levels was observed only for ASOs with perfect complementarity to certain positions of the target mRNA, but not with control ASOs without complementarity or with ASOs that base pair with different positions of the same mRNA, as seen for *RNASEH1*, *LDLR*, and *ACP1* mRNAs. In addition, reducing the hybridization potential by introducing mismatches or shifting the target sites in an mRNA altered ASO effects. Importantly, the ASOs targeting *RNASEH1* and *LDLR* mRNAs shifted the targeted mRNAs, but not *PTEN* mRNA, from monosomes toward polysomes, indicating a target-specific increase in translation. Moreover, the levels of multiple control proteins used in this study were not affected by altering ASO concentrations, whereas the levels of targeted proteins responded in an ASO dose-dependent manner, suggesting that the increased levels of targeted proteins were not caused by ASO effects on global translation.

The ASOs specifically increased protein levels of targeted genes in a hybridization-dependent manner with minor off-target effects on the expression of other genes. The specificity was due to the highly position-dependent effect of ASOs that bind to the mRNAs. The ASO specificity is reflected by the observations that ASOs that perfectly base pair with other regions of the same mRNA did not increase the levels of the targeted proteins and that ASOs that imperfectly base pair with an off-target mRNA did not affect the level of that protein. These target- and position-specific effects of ASOs suggest that the observed protein increase was not due to global effects on translation. In addition, the ASO specificity was also supported by the results from microarray and proteomics studies. Although microarray analyses revealed that some mRNAs exhibited altered expression levels, these could be false-positive detections, as the expression levels of those mRNAs are low and changes were not validated by a more accurate qRT-PCR assay for several tested mRNAs. In addition, results from proteomics analyses indicate that very few proteins seemed to be affected by transfection of the ASO.

Evidence suggests that ASOs targeting the inhibitory regions increase protein levels by enhancing translation. First, the mRNA levels of the targeted genes were not increased by the ASOs. Second, nascent protein levels were increased, as shown for LDLR. Third, upon treatment with ASOs targeting inhibitory regions, the targeted mRNAs shifted from monosomes toward polysomes, as shown for the *RNASEH1* and *LDLR* mRNAs. Finally, for both *ACP1* and *LDLR* mRNAs more mRNA was co-isolated with translation factor eIF4A after specific ASO treatment. Together, these observations strongly suggest that the ASOs enhance translation of the target mRNAs.

5′ UTR inhibitory elements in different mRNAs can influence translation by various mechanisms, including the well-demonstrated secondary structures that can inhibit translation in a position- and stability-dependent manner (44,47). In this study, we found that more eIF4A and eIF2a proteins associated with *ACP1* mRNA upon ASO binding, and more *ACP1* and *LDLR* mRNAs were co-isolated with eIF4A upon ASO treatment. Thus, it is possible that the potential increase in the length of single-stranded region

near the 5′ cap of the mRNA induced by ASO hybridization enhances the recruitment of translation initiation factors, which may prefer to bind to single-stranded RNA regions versus structured regions (77). This possibility is supported by previous findings that binding of PIC or eIF4B was inhibited by stem structures near the cap, but not by structures that are not close to the cap (44,49). Once the PIC is efficiently docked onto the mRNA, the ASO/mRNA duplex might be disrupted and the ASO be removed by the scanning process, as the PIC is able to melt certain structure (not too stable) once it bound to mRNA (33,44).

It is possible that helicases are involved in the potential ASO removal from mRNA. This is supported by the observations that the ASO effect was dependent on the helicase DHX29, which has been shown to resolve 5′ UTR structures (72), and by our finding that the tested *ACP1* ASO did not cause significant structural changes in the mRNA target in cells. We note that the 5′ UTR structure may be dynamic and not stable, and in heterogeneity, due to the constant scanning by the PIC along the 5′ UTR and different translation stages of each mRNA molecule at a given time (73). Thus, although protein levels are increased by ASOs targeting both uORFs and potential inhibitory structures, the underlying mechanisms appear to be different. The uORF ASOs inhibit translation initiation from the uORF, redirecting translation initiation to the AUG of the pORF. In contrast, the ASOs targeting potential structural elements may alter mRNA structures or impede binding of *trans*-acting inhibitory factors and thus enhance the recruitment of initiation factors and perhaps enhance scanning as well.

The affinity of ASOs for a particular mRNA must be optimized. The affinity for the mRNA needs to be high enough to result in invasion of the intramolecular mRNA structure, but the interaction cannot be so stable that the duplex between mRNA and ASO cannot be unwound by PIC, as a strong stem structure can block PIC scanning even if placed far from the 5′ cap (44). Optimal length and extent of chemical modification need to be experimentally determined for each mRNA. In experiments described here both 16-mer and 18-mer 2′-*O*-Me-modified ASOs were functional. Chemical modifications can alter affinity and are necessary for use in animals. The design, chemical modification, the pharmacokinetics and pharmacodynamics of ASOs have been well studies (4,64). For example, the PS modification reduces melting temperatures of hybrid duplexes by about 0.5°C per modification compared with PO backbone, whereas 2′-*O*-Me and 2′-cEt modifications increase melting temperatures by approximately 0.5 and 3 to 5°C per modification, respectively. Therefore, combinations of ASO lengths and chemical modifications should be evaluated. When chemical modifications that enabled systemic delivery were used, an ASO targeting a potential structure region of *ACP1* 5′ UTR increased the protein levels in mice after subcutaneous injection without the need for formulation.

Since uORFs are present in ∼50% of human mRNAs and many mRNAs also contain potential structural elements (30,31), ASO-based agents designed to target structural inhibitory regions or uORFs can be used to specifically increase levels of endogenous proteins encoded by many genes. We note that some secondary structures can be predicted computationally, the inhibitory effect of predicted structures in 5′ UTRs must be experimentally determined. Nonetheless, the approach validated here will be a valuable tool for research and for the development of 'agonist-like' drugs. This approach clearly has therapeutic potential as we showed increased LDL uptake in cells treated with an ASO targeting *LDLR* mRNA. Although the increase in the level of the targeted proteins was modest, it was clearly of functional impact in cells with normal expression of LDLR. A greater change is expected in patients who have low levels of expression of LDLR. For many applications, increasing the level of a protein by 50–170%, the range observed here, would produce meaningful phenotypic changes, as exemplified for SMN and CTLA-4 proteins (9,10).

SUPPLEMENTARY DATA

Supplementary Data are available at NAR Online.

REFERENCES

1. Wilson,J.A. and Richardson,C.D. (2006) Future promise of siRNA and other nucleic acid based therapeutics for the treatment of chronic HCV. *Infect. Disord. Drug Targets*, **6**, 43–56.
2. Lu,P.Y., Xie,F. and Woodle,M.C. (2005) In vivo application of RNA interference: from functional genomics to therapeutics. *Adv. Genet.*, **54**, 117–142.
3. Bennett,C.F. and Swayze,E.E. (2010) RNA targeting therapeutics: molecular mechanisms of antisense oligonucleotides as a therapeutic platform. *Annu. Rev. Pharmacol. Toxicol.*, **50**, 259–293.
4. Crooke,S.T.V.T.A., Lima,W.F. and Wu,H.-J. (2008) In: Crooke,ST (ed). *Antisense Drug Technology - Principles, Strategies, and Applications*. 2nd edn. CRC Press, Boca Raton, pp. 3–46.
5. Rossbach,M. (2010) Small non-coding RNAs as novel therapeutics. *Curr. Mol. Med.*, **10**, 361–368.
6. Segalat,L. (2007) Loss-of-function genetic diseases and the concept of pharmaceutical targets. *Orphanet. J. Rare Dis.*, **2**, 1–6.
7. Crosby,J., Peloso,G.M., Auer,P.L., Crosslin,D.R., Stitziel,N.O., Lange,L.A., Lu,Y., Tang,Z.Z., Zhang,H., Hindy,G. *et al.* (2014) Loss-of-function mutations in APOC3, triglycerides, and coronary disease. *N. Engl. J. Med.*, **371**, 22–31.
8. Hoyng,S.A., de Winter,F., Tannemaat,M.R., Blits,B., Malessy,M.J. and Verhaagen,J. (2015) Gene therapy and peripheral nerve repair: a perspective. *Front. Mol. Neurosci.*, **8**, 1–9.
9. Hua,Y., Vickers,T.A., Baker,B.F., Bennett,C.F. and Krainer,A.R. (2007) Enhancement of SMN2 exon 7 inclusion by antisense oligonucleotides targeting the exon. *PLoS Biol.*, **5**, e73.
10. Mourich,D.V., Oda,S.K., Schnell,F.J., Crumley,S.L., Hauck,L.L., Moentenich,C.A., Marshall,N.B., Hinrichs,D.J. and Iversen,P.L. (2014) Alternative splice forms of CTLA-4 induced by antisense mediated splice-switching influences autoimmune diabetes susceptibility in NOD mice. *Nucleic Acid Ther.*, **24**, 114–126.

11. Nomakuchi,T.T., Rigo,F., Aznarez,I. and Krainer,A.R. (2016) Antisense oligonucleotide-directed inhibition of nonsense-mediated mRNA decay. *Nat. Biotech.*, **34**, 164–166.

12. Pearson,S., Jia,H. and Kandachi,K. (2004) China approves first gene therapy. *Nat. Biotech.*, **22**, 3–4.

13. Leader,B., Baca,Q.J. and Golan,D.E. (2008) Protein therapeutics: a summary and pharmacological classification. *Nat. Rev. Drug Discov.*, **7**, 21–39.

14. Meng,L., Ward,A.J., Chun,S., Bennett,C.F., Beaudet,A.L. and Rigo,F. (2015) Towards a therapy for Angelman syndrome by targeting a long non-coding RNA. *Nature*, **518**, 409–412.

15. Muller,P.P. and Trachsel,H. (1990) Translation and regulation of translation in the yeast Saccharomyces cerevisiae. *Eur. J. Biochem.*, **191**, 257–261.

16. van der Velden,A.W. and Thomas,A.A. (1999) The role of the 5′ untranslated region of an mRNA in translation regulation during development. *Int. J. Biochem. Cell Biol.*, **31**, 87–106.

17. Jackson,R.J., Hellen,C.U. and Pestova,T.V. (2010) The mechanism of eukaryotic translation initiation and principles of its regulation. *Nat. Rev. Mol. Cell Biol.*, **11**, 113–127.

18. Chu,D. and von der Haar,T. (2012) The architecture of eukaryotic translation. *Nucleic Acids Res.*, **40**, 10098–10106.

19. Araujo,P.R., Yoon,K., Ko,D., Smith,A.D., Qiao,M., Suresh,U., Burns,S.C. and Penalva,L.O. (2012) Before it gets started: regulating translation at the 5′ UTR. *Comp. Funct. Genomics*, **2012**, 1–9.

20. Baird,S.D., Turcotte,M., Korneluk,R.G. and Holcik,M. (2006) Searching for IRES. *RNA*, **12**, 1755–1785.

21. Jackson,R.J. (2005) Alternative mechanisms of initiating translation of mammalian mRNAs. *Biochem. Soc. Trans.*, **33**, 1231–1241.

22. Alekhina,O.M. and Vassilenko,K.S. (2012) Translation initiation in eukaryotes: versatility of the scanning model. *Biochemistry (Mosc.)*, **77**, 1465–1477.

23. Sonenberg,N. and Hinnebusch,A.G. (2009) Regulation of translation initiation in eukaryotes: mechanisms and biological targets. *Cell*, **136**, 731–745.

24. Kozak,M. (1980) Evaluation of the "scanning model" for initiation of protein synthesis in eucaryotes. *Cell*, **22**, 7–8.

25. Kozak,M. (2002) Pushing the limits of the scanning mechanism for initiation of translation. *Gene*, **299**, 1–34.

26. Hinnebusch,A.G. (2014) The scanning mechanism of eukaryotic translation initiation. *Annu. Rev. Biochem.*, **83**, 779–812.

27. Hinnebusch,A.G., Ivanov,I.P. and Sonenberg,N. (2016) Translational control by 5′-untranslated regions of eukaryotic mRNAs. *Science*, **352**, 1413–1416.

28. Ringner,M. and Krogh,M. (2005) Folding free energies of 5′-UTRs impact post-transcriptional regulation on a genomic scale in yeast. *PLoS Comput. Biol.*, **1**, e72.

29. Liang,X.-h., Shen,W., Sun,H., Migawa,M.T., Vickers,T.A. and Crooke,S.T. (2016) Translation efficiency of mRNAs is increased by antisense oligonucleotides targeting upstream open reading frames. *Nat. Biotech.*, **34**, 875–880.

30. Calvo,S.E., Pagliarini,D.J. and Mootha,V.K. (2009) Upstream open reading frames cause widespread reduction of protein expression and are polymorphic among humans. *Proc. Natl. Acad. Sci. U.S.A.*, **106**, 7507–7512.

31. Lee,S., Liu,B., Lee,S., Huang,S.X., Shen,B. and Qian,S.B. (2012) Global mapping of translation initiation sites in mammalian cells at single-nucleotide resolution. *Proc. Natl. Acad. Sci. U.S.A.*, **109**, E2424–E2432.

32. Pickering,B.M. and Willis,A.E. (2005) The implications of structured 5′ untranslated regions on translation and disease. *Semin. Cell Dev. Biol.*, **16**, 39–47.

33. Kozak,M. (1991) Structural features in eukaryotic mRNAs that modulate the initiation of translation. *J. Biol. Chem.*, **266**, 19867–19870.

34. Davuluri,R.V., Suzuki,Y., Sugano,S. and Zhang,M.Q. (2000) CART classification of human 5′ UTR sequences. *Genome Res.*, **10**, 1807–1816.

35. Bugaut,A. and Balasubramanian,S. (2012) 5′-UTR RNA G-quadruplexes: translation regulation and targeting. *Nucleic Acids Res.*, **40**, 4727–4741.

36. Lukowski,S.W., Rothnagel,J.A. and Trezise,A.E. (2015) CFTR mRNA expression is regulated by an upstream open reading frame and RNA secondary structure in its 5′ untranslated region. *Hum. Mol. Genet.*, **24**, 899–912.

37. Rouleau,S.G., Beaudoin,J.D., Bisaillon,M. and Perreault,J.P. (2015) Small antisense oligonucleotides against G-quadruplexes: specific mRNA translational switches. *Nucleic Acids Res.*, **43**, 595–606.

38. Suzuki,Y., Holmes,J.B., Cerritelli,S.M., Sakhuja,K., Minczuk,M., Holt,I.J. and Crouch,R.J. (2010) An upstream open reading frame and the context of the two AUG codons affect the abundance of mitochondrial and nuclear RNase H1. *Mol. Cell. Biol.*, **30**, 5123–5134.

39. Kozak,M. (1986) Influences of mRNA secondary structure on initiation by eukaryotic ribosomes. *Proc. Natl. Acad. Sci. U.S.A.*, **83**, 2850–2854.

40. Lawson,T.G., Ray,B.K., Dodds,J.T., Grifo,J.A., Abramson,R.D., Merrick,W.C., Betsch,D.F., Weith,H.L. and Thach,R.E. (1986) Influence of 5′ proximal secondary structure on the translational efficiency of eukaryotic mRNAs and on their interaction with initiation factors. *J. Biol. Chem.*, **261**, 13979–13989.

41. Sagliocco,F.A., Vega Laso,M.R., Zhu,D., Tuite,M.F., McCarthy,J.E. and Brown,A.J. (1993) The influence of 5′-secondary structures upon ribosome binding to mRNA during translation in yeast. *J. Biol. Chem.*, **268**, 26522–26530.

42. Curran,J.A. and Weiss,B. (2016) What Is the Impact of mRNA 5′ TL heterogeneity on translational start site selection and the mammalian cellular phenotype? *Front. Genet.*, **7**, 1–12.

43. Dvir,S., Velten,L., Sharon,E., Zeevi,D., Carey,L.B., Weinberger,A. and Segal,E. (2013) Deciphering the rules by which 5′-UTR sequences affect protein expression in yeast. *Proc. Natl. Acad. Sci. U.S.A.*, **110**, E2792–E2801.

44. Kozak,M. (1989) Circumstances and mechanisms of inhibition of translation by secondary structure in eucaryotic mRNAs. *Mol. Cell. Biol.*, **9**, 5134–5142.

45. Oliveira,C.C., van den Heuvel,J.J. and McCarthy,J.E. (1993) Inhibition of translational initiation in Saccharomyces cerevisiae by secondary structure: the roles of the stability and position of stem-loops in the mRNA leader. *Mol. Microbiol.*, **9**, 521–532.

46. Gray,N.K. and Hentze,M.W. (1994) Regulation of protein synthesis by mRNA structure. *Mol. Biol. Rep.*, **19**, 195–200.

47. Babendure,J.R., Babendure,J.L., Ding,J.H. and Tsien,R.Y. (2006) Control of mammalian translation by mRNA structure near caps. *RNA*, **12**, 851–861.

48. Kozak,M. (2005) Regulation of translation via mRNA structure in prokaryotes and eukaryotes. *Gene*, **361**, 13–37.

49. Pelletier,J. and Sonenberg,N. (1985) Photochemical cross-linking of cap binding proteins to eucaryotic mRNAs: effect of mRNA 5′ secondary structure. *Mol. Cell. Biol.*, **5**, 3222–3230.

50. Koller,E., Vincent,T.M., Chappell,A., De,S., Manoharan,M. and Bennett,C.F. (2011) Mechanisms of single-stranded phosphorothioate modified antisense oligonucleotide accumulation in hepatocytes. *Nucleic Acids Res.*, **39**, 4795–4807.

51. Zuker,M. (2003) Mfold web server for nucleic acid folding and hybridization prediction. *Nucleic Acids Res.*, **31**, 3406–3415.

52. Lorenz,R., Bernhart,S.H., Honer Zu Siederdissen,C., Tafer,H., Flamm,C., Stadler,P.F. and Hofacker,I.L. (2011) ViennaRNA Package 2.0. *Algorithms Mol. Biol.*, **6**, 1–14.

53. O'Leary,N.A., Wright,M.W., Brister,J.R., Ciufo,S., Haddad,D., McVeigh,R., Rajput,B., Robbertse,B., Smith-White,B., Ako-Adjei,D. *et al.* (2016) Reference sequence (RefSeq) database at NCBI: current status, taxonomic expansion, and functional annotation. *Nucleic Acids Res.*, **44**, D733–745.

54. Liang,X.H., Hart,C.E. and Crooke,S.T. (2013) Transfection of siRNAs can alter miRNA levels and trigger non-specific protein degradation in mammalian cells. *Biochim. Biophys. Acta*, **1829**, 455–468.

55. Liang,X.H. and Crooke,S.T. (2011) Depletion of key protein components of the RISC pathway impairs pre-ribosomal RNA processing. *Nucleic Acids Res.*, **39**, 4875–4889.

56. Liang,X.H., Vickers,T.A., Guo,S. and Crooke,S.T. (2011) Efficient and specific knockdown of small non-coding RNAs in mammalian cells and in mice. *Nucleic Acids Res.*, **39**, e13.

57. Chiang,M.Y., Chan,H., Zounes,M.A., Freier,S.M., Lima,W.F. and Bennett,C.F. (1991) Antisense oligonucleotides inhibit intercellular adhesion molecule 1 expression by two distinct mechanisms. *J. Biol. Chem.*, **266**, 18162–18171.

58. Tripathi,V., Ellis,J.D., Shen,Z., Song,D.Y., Pan,Q., Watt,A.T., Freier,S.M., Bennett,C.F., Sharma,A., Bubulya,P.A. *et al.* (2010) The nuclear-retained noncoding RNA MALAT1 regulates alternative splicing by modulating SR splicing factor phosphorylation. *Mol. Cell*, **39**, 925–938.

59. Khan,A.A., Betel,D., Miller,M.L., Sander,C., Leslie,C.S. and Marks,D.S. (2009) Transfection of small RNAs globally perturbs gene regulation by endogenous microRNAs. *Nat. Biotech.*, **27**, 549–555.

60. Zheng,Y., Cretoiu,D., Yan,G., Cretoiu,S.M., Popescu,L.M., Fang,H. and Wang,X. (2014) Protein profiling of human lung telocytes and microvascular endothelial cells using iTRAQ quantitative proteomics. *J. Cell. Mol. Med.*, **18**, 1035–1059.

61. Van der Horst,D.J., Roosendaal,S.D. and Rodenburg,K.W. (2009) Circulatory lipid transport: lipoprotein assembly and function from an evolutionary perspective. *Mol. Cell. Biochem.*, **326**, 105–119.

62. Fitzgerald,K., Frank-Kamenetsky,M., Shulga-Morskaya,S., Liebow,A., Bettencourt,B.R., Sutherland,J.E., Hutabarat,R.M., Clausen,V.A., Karsten,V., Cehelsky,J. *et al.* (2014) Effect of an RNA interference drug on the synthesis of proprotein convertase subtilisin/kexin type 9 (PCSK9) and the concentration of serum LDL cholesterol in healthy volunteers: a randomised, single-blind, placebo-controlled, phase 1 trial. *Lancet*, **383**, 60–68.

63. Boiziau,C., Kurfurst,R., Cazenave,C., Roig,V., Thuong,N.T. and Toulme,J.J. (1991) Inhibition of translation initiation by antisense oligonucleotides via an RNase-H independent mechanism. *Nucleic Acids Res.*, **19**, 1113–1119.

64. Geary,R.S., Norris,D., Yu,R. and Bennett,C.F. (2015) Pharmacokinetics, biodistribution and cell uptake of antisense oligonucleotides. *Adv. Drug Delivery Rev.*, **87**, 46–51.

65. Bennett,C.F. (2006) In: Crooke,ST (ed). *Antisense Drug Technology - Principles, Strategies, and Applications*. CRC Press, Boca Raton, pp. 273–304.

66. Seth,P.P., Vasquez,G., Allerson,C.A., Berdeja,A., Gaus,H., Kinberger,G.A., Prakash,T.P., Migawa,M.T., Bhat,B. and Swayze,E.E. (2010) Synthesis and biophysical evaluation of 2′,4′-constrained 2′O-methoxyethyl and 2′,4′-constrained 2′O-ethyl nucleic acid analogues. *J. Org. Chem.*, **75**, 1569–1581.

67. Baim,S.B. and Sherman,F. (1988) mRNA structures influencing translation in the yeast Saccharomyces cerevisiae. *Mol. Cell. Biol.*, **8**, 1591–1601.

68. Bettany,A.J., Moore,P.A., Cafferkey,R., Bell,L.D., Goodey,A.R., Carter,B.L. and Brown,A.J. (1989) 5′-secondary structure formation, in contrast to a short string of non-preferred codons, inhibits the translation of the pyruvate kinase mRNA in yeast. *Yeast*, **5**, 187–198.

69. Cigan,A.M., Pabich,E.K. and Donahue,T.F. (1988) Mutational analysis of the HIS4 translational initiator region in Saccharomyces cerevisiae. *Mol. Cell. Biol.*, **8**, 2964–2975.

70. Rao,C.D., Pech,M., Robbins,K.C. and Aaronson,S.A. (1988) The 5′ untranslated sequence of the c-sis/platelet-derived growth factor 2 transcript is a potent translational inhibitor. *Mol. Cell. Biol.*, **8**, 284–292.

71. Johannes,G. and Berger,F.G. (1992) Alterations in mRNA translation as a mechanism for the modification of enzyme synthesis during evolution. The ornithine decarboxylase model. *J. Biol. Chem.*, **267**, 10108–10115.

72. Pisareva,V.P., Pisarev,A.V., Komar,A.A., Hellen,C.U. and Pestova,T.V. (2008) Translation initiation on mammalian mRNAs with structured 5′UTRs requires DExH-box protein DHX29. *Cell*, **135**, 1237–1250.

73. Rouskin,S., Zubradt,M., Washietl,S., Kellis,M. and Weissman,J.S. (2014) Genome-wide probing of RNA structure reveals active unfolding of mRNA structures in vivo. *Nature*, **505**, 701–705.

74. Evers,M.M., Toonen,L.J.A. and van Roon-Mom,W.M.C. (2015) Antisense oligonucleotides in therapy for neurodegenerative disorders. *Adv. Drug Delivery Rev.*, **87**, 90–103.

75. Johnstone,T.G., Bazzini,A.A. and Giraldez,A.J. (2016) Upstream ORFs are prevalent translational repressors in vertebrates. *EMBO J.*, **35**, 706–723.

76. Wang,L. and Wessler,S.R. (2001) Role of mRNA secondary structure in translational repression of the maize transcriptional activator Lc(1,2). *Plant Physiol.*, **125**, 1380–1387.

77. Lorsch,J.R. and Herschlag,D. (1998) The DEAD box protein eIF4A. 1. A minimal kinetic and thermodynamic framework reveals coupled binding of RNA and nucleotide. *Biochemistry*, **37**, 2180–2193.